Accepted Manuscript

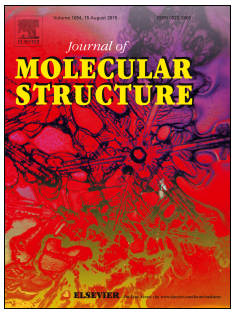

Synthesis, characterization, theoretical study and biological activity of Schiff base nanomaterial analogues

G.G. Mohamed, W.H. Mahmoud, M.A. Diab, A.Z. El-Sonbati, S.Y. Abbas

PII: S0022-2860(19)30007-9

DOI: https://doi.org/10.1016/j.molstruc.2019.01.007

Reference: MOLSTR 26058

To appear in: *Journal of Molecular Structure*

Received Date: 10 November 2018

Revised Date: 2 January 2019

Accepted Date: 2 January 2019

Please cite this article as: G.G. Mohamed, W.H. Mahmoud, M.A. Diab, A.Z. El-Sonbati, S.Y. Abbas, Synthesis, characterization, theoretical study and biological activity of Schiff base nanomaterial analogues, *Journal of Molecular Structure* (2019), doi: https://doi.org/10.1016/j.molstruc.2019.01.007.

Synthesis, characterization, theoretical study and biological activity of Schiff base nanomaterial analogues

G.G. Mohamed[1, 2], W.H. Mahmoud[1], M.A. Diab[3], A.Z. El-Sonbati[3,*], S. Y. Abbas[3]

[1]Chemistry Department, Faculty of Science, Cairo University, Giza 12613, Egypt

[2] Egypt Nanotechnology Center, Cairo University, El-Sheikh Zayed, 6th October, 12588, Egypt

[3]Chemistry Department, Faculty of Science, Damietta University, Egypt

Abstract

The ligand named (H_2L: 2,2'-((1E,1'E)-(1,3 phenylene bis (azanylylidene)) bis (methanylylidene))diphenol) was prepared from the reaction of *m*-phenylenediamine and 2-hydroxybenzaldehyde. A series of Co(II), Ni(II), Cu(II), Cr(III), Mn(II), Fe(III), Zn(II) and Cd(II) complexes of the ligand were prepared and characterized using different physicochemical techniques. The infrared spectral data showed that the chelation occurs through the deprotonated phenolic oxygen and azomethine nitrogen atoms of the ligand. The data showed that the complexes have composition of ML type. An octahedral geometry around the central metal ions in the complexes was suggested. The molecular structures of the ligand and its metal complexes were optimized theoretically. Scanning electron microscope micrograph proved that the ligand and its Fe(III) complex were formed in nano size. The synthesized Schiff base ligand and its complexes have been screened for antimicrobial activities against bacterial species and fungi. A comparative study of the inhibition zones of the ligand and its metal complexes indicates that most complexes exhibit higher antibacterial and antifungal effect against bacterial species than the free ligand. The molecular docking is used to predict the efficiency of binding between Schiff base ligand and both receptors of crystal structure of *Escherichia coli* (3T88) and crystal structure of *Staphylococcus aureus* (3Q8U).

Keywords: Schiff base; Complexes; Biological activity; Molecular docking; Thermal analysis.

*Corresponding author: E-mail address: elsonbatisch@yahoo.com (A.Z. El-Sonbati)

1. Introduction

Much attention has been recently paid to the study of Schiff base complexes with transition metals of biological, environmental, industrial and pharmaceutical interests [1]. Recently, much research on macrocyclic complexes have been focused on species containing the first-row transition metal ions and tetradentate ligands [2]. As known, the third most abundant metal ions in human body are iron, zinc and copper and these metal ions play critical and crucial roles in many biological processes such as RNA and DNA synthesis [3], gene expression and enzyme regulation [4], the structural and functional enhancement of proteins [5]. Due to their importance in biological processes, Cu(II) complexes synthesis and activity studies have been the focus from different perspectives [6]. Moreover, Schiff base amino acid complexes of first-row transition metals specially Cu(II) were reported to exhibit fungicidal, bactericidal, antiviral and antitubercular activity [7]. Schiff base amino acid complexes of Cu(II) have received much attention due to their high biological activity [8]. In some cases, Schiff bases and its metal complexes are potentially used as anticancer drugs [9]. Moreover, these compounds show many important biological activities such as antimicrobial and antifungal [10]. Schiff bases appear to be important intermediates in a number of enzymatic reactions involving enzyme interaction with an amino or a carbonyl group of a substrate. In bioinorganic chemistry, the interest in the Schiff base complexes derives from their ability to provide synthetic models for metal-containing sites in metalloproteins and to contribute to developments in medicinal chemistry. Thus, Schiff bases and their complexes have a variety of applications in biological, clinical, and analytical fields [11]. Furthermore, complexes of transition metals, which involve derivatives of salicylaldehyde and diamine, have received considerable attention. This is because of their potential as catalysts for the insertion of oxygen into an organic substrate [12].

Schiff base complexes have been considered to be among the most important stereo chemical models in main group and transition metal coordination chemistry due to their preparative accessibility and structural variety [1,13-15]. Metal complexes of Schiff bases have a wide variety of biological applications such as antitumor, antimicrobial and antioxidant activities. Transition metal complexes of Schiff bases are of interest due to their appreciable biological activities and commercial importance [14-21]

In this paper, Schiff base ligand 2,2'-((1E,1'E)-(1,3 phenylene bis (azanylylidene)) bis (methanylylidene))diphenol) (H_2L) derived from the reaction of *m*-phenylenediamine and 2-hydroxybenzaldehyde was synthesized and characterized. The interaction of H_2L with different metal ions was prepared and characterized by spectroscopic and molecular docking methods. In addition to the molecular structures of the Schiff base ligand (H_2L) and its metal complexes were optimized theoretically and the quantum chemical parameters were calculated and discussed. The new compounds were tested for their antimicrobial and antifungal activities against different organisms and compared with the standard antibacterial and antifungal drugs. The calculated binding energy values of the receptors (*Escherichia coli* (3T88) and *Staphylococcus aureu* (3Q8U)) for Schiff base ligand (H_2L) compared to antimicrobial activities against *Escherichia coli* (Gram (-) bacteria) and *Staphylococcus aureus* (Gram (+) bacteria).

2. Experimental

2.1. Materials and reagents

All chemicals used included 2-hydroxybenzaldehyde, *m*-phenylenediamine, $CrCl_3 \cdot 6H_2O$, $MnCl_2 \cdot 4H_2O$, $FeCl_3$, $CoCl_2 \cdot 6H_2O$ and $CuCl_2.2H_2O$ were baught from Sigma. They were purified by standard methods. $ZnCl_2$ (Strem Chemicals) , $CdCl_2$ (Sigma- Aldrich) $NiCl_2.6H_2O$ (BDH Chemical Ltd),. They were of the analytical reagent grade (AR), and of highest purity available. The organic solvents such as absolute ethyl alcohol and dimethylformamide (DMF) were either spectroscopic pure from BDH Chemical Ltd or purified by the recommended methods [22].

2.2. Instruments

Microanalyses of carbon, hydrogen and nitrogen were carried out at the Microanalytical Center, Cairo University, Egypt, using CHNS-932 (LECO) Vario Elemental Analyzer. FT-IR spectra were recorded on a Perkin-Elmer 1650 spectrometer (4000–400 cm^{-1}) in KBr pellets. Electronic spectra were recorded at room temperature on a Shimadzu 3101pc spectrophotometer as solutions in DMF. ^1H NMR spectra, as a solution in DMSO- d_6 were recorded on a 300 MHz Varian-Oxford Mercury at room temperature using TMS as an internal standard.

Mass spectra were recorded by the EI technique at 70 eV using MS-5988 GS-MS Hewlett-Packard instrument at the Microanalytical Center, National Center for Research, Egypt. The molar magnetic susceptibility was measured on powdered samples using the Faraday method. The diamagnetic corrections were made by Pascal's constant and $Hg[Co(SCN)_4]$ was used as a calibrant. Molar conductivities of 10^{-3} M solutions of the solid complexes in DMF were measured on by using Jenway 4010 conductivity meter. The scanning electron microscopic (SEM) image of the complexes was recorded by using SEM model Quanta 250 FEG (Field Emission Gun) attached with EDX Unit (Energy Dispersive X-ray Analyses), with accelerating voltage 30 K.V. magnification 14x up to 1000000 and resolution for Gun.1n, National Research Center, Egypt. The thermogravimetric analysis (TGA) was carried out from room temperature to 1000 °C using a Shimadzu TG-50H thermal analyzer. The antimicrobial activities were carried out at the Microanalytical center, Cairo University, Egypt.

Perkin Elmer ChemBio 3D software was used in calculating the optimized geometry by HF method with 3–21 G basis set [23-25] to obtain the most stable structure.

Molecular docking calculations were performed using Docking Server [26-28]. The ligand atoms have Gasteiger partial charges. Rotatable bonds were defined. Non-polar hydrogen atoms were added. Docking calculations were carried out on LYASE / LYASE INHIBITOR Crystal structure of *Escherichia coli* MenB in complex with substrate analogue OSB-NCoA (3T88) and TRANSFERASE Crystal structure of *Staphylococcus aureus* nucleoside diphosphate kinase complexed with ADP (3Q8U) proteins model [28-30].

2.3. Synthesis of ligand (H_2L)

H_2L Schiff base ligand was synthesized by condensation of *m*-phenylenediamine with 2-hydroxybenzaldehyde (Scheme 1). A solution of 2-hydroxybenzaldehyde (74 mmol, 9.04 g, 7.74 ml) dissolved in ethanol was added dropwise to *m*-phenylenediamine (37 mmol, 4g) dissolved in ethanol. The resulting mixture was stirred under reflux for about 3 h at temperature (100-150 ^{o}C) which an orange solid compound was separated. It was filtered, recrystallized and washed with diethylether and dried in vacuum.

Yield 52.33 %; m.p. 130°C; yellowish green solid. Anal. Calcd. for $C_{20}H_{16}N_2O_2$ (%): C, 75.95; H, 5.06; N, 8.86. Found (%): C, 75.93; H, 5.05; N, 8.85. FT-IR (cm^{-1}): phenolic υ(OH) 3438, azomethine υ(C=N) 1617, υ(C-N) 1386, υ(C-O) phenolic 1276. ^{1}H NMR (300 MHz, DMSO-d*6*, δ, ppm): 13.00 (s, 2H, OH phenolic), 9.05 (s, 2H, CH=N), 6.91-8.71 (m, 12H, Ar H). λ_{max} (cm^{-1}): 46082 and 40650 (π–π*), 30030 (n–π*).

2.4. Synthesis of complexes of H_2L

The complexes were prepared by the addition of hot solution (60 °C) of the appropriate metal chlorides (1.266 mmol) in ethanol to the hot solution (60 °C) of the ligand (0.4g, 1.266 mmol) in a mixture of ethanol and DMF by molar ratio (2:1 v/v). The resulting mixture was stirred under reflux for two hours whereupon the complexes precipitated. They were collected by filtration, washed with hot ethanol and purified by washing several times with diethyl ether. The analytical data for C, H and N were repeated twice.

$[Cr(L)(Cl)(OH_2)].H_2O$ (1)

Yield 72.28 %; green solid, m.p. 118 °C. Anal. Calcd. for $Cr(C_{20}H_{18}ClN_2O_4)$ (%): C, 54.86; H, 4.12; N, 6.40; Cr, 11.89. Found (%): C, 54.87; H, 4.11; N, 6.41; Cr, 11.88. FT-IR (cm^{-1}): phenolic υ(OH) 3319, azomethine υ(C=N) 1645, υ(H_2O) stretching bands of coordinated water 932 and 896, υ(M-O) stretching bands of coordinated water 519, metal–nitrogen bond υ(M-N) 479. Molar conductivity(10^{-3} M, DMSO): 43.0 Ω^{-1} cm^2 mol^{-1}. μ_{eff} = 3.58 B.M. λ_{max}(cm^{-1}): 46948 and 40816 (π–π*), 29850 (n–π*).

$[Mn(L)(OH_2)_2].H_2O$ (2)

Yield 73.82 %; yellowish green solid, m.p. 90 °C. Anal. Calcd. for $Mn(C_{20}H_{20}N_2O_5)$ (%): C, 56.74; H, 4.73; N, 6.62; Mn, 12.99. Found (%): C, 56.72; H, 4.74; N, 6.63; Mn, 12.98. FT-IR (cm^{-1}): phenolic υ(OH) 3426, azomethine υ(C=N) 1647, υ(C-N) 1378, phenolic υ(C-O) 1275, υ(H_2O) stretching bands of coordinated water 960 and 869, υ(M-O) stretching bands of coordinated water 530, metal-oxygen bond υ(M-O) 543, metal-nitrogen bond υ(M-N) 450. Molar conductivity(10^{-3} M, DMSO): 33.8 Ω^{-1} cm^2 mol^{-1}. μ_{eff} = 5.43 B.M. λ_{max} (cm^{-1}):: 46082 and 41152 (π–π*), 29850 (n–π*).

[Fe(L)(OH$_2$)$_2$].Cl (3)

Yield 60.89 %; black solid, m.p. 121 °C. Anal. Calcd. for Fe($C_{20}H_{18}ClN_2O_4$) (%): C, 54.37; H, 4.08; N, 6.34; Fe, 12.68. Found (%): C, 54.35; H, 4.10; N, 6.35; Fe, 12.67. FT-IR (cm^{-1}): phenolic υ(OH) 3429, azomethine υ(C=N) 1640, υ(C-N) 1371, phenolic υ(C-O) 1284, υ(H_2O) stretching bands of coordinated water 958 and 872, υ(M-O) stretching bands of coordinated water 570, metal-oxygen bond υ(M-O) 580, metal-nitrogen bond υ(M-N) 455. Molar conductivity(10^{-3} M, DMSO): 63.9 Ω^{-1} cm^2 mol^{-1}. μ_{eff} = 5.17 B.M. λ_{max} (cm^{-1}): 46082 and 41152 (π–π*), 29850 (n–π*).

[Co(L)(OH$_2$)$_2$].H$_2$O (4)

Yield 66.66 %; blue solid, m.p. 120 °C. Anal. Calcd. for Co($C_{20}H_{20}N_2O_5$) (%): C, 56.22; H, 4.69; N, 6.56; Co, 13.80. Found (%): C, 56.23; H, 4.68; N, 6.57; Co, 13.79. FT-IR (cm^{-1}): phenolic υ(OH) 3428, azomethine υ(C=N) 1646, υ(C-N) 1382, phenolic υ(C-O) 1238, υ(H_2O) stretching bands of coordinated water 937 and 853, υ(M-O) stretching bands of coordinated water 538, metal-oxygen bond υ(M-O) 579, metal-nitrogen bond υ(M-N) 459. Molar conductivity(10^{-3} M, DMSO): 46.8 Ω^{-1} cm^2 mol^{-1}. μ_{eff} = 5.18 B.M. λ_{max} (cm^{-1}): 46082 and 41152 (π–π*), 29850 (n–π*).

[Ni(L)(OH$_2$)$_2$].H$_2$O (5)

Yield 37.05 %; yellowish green solid, m.p. 90 °C. Anal. Calcd. for Ni($C_{20}H_{20}N_2O_5$) (%): C, 56.25; H, 4.70; N, 6.56; Ni, 13.75. Found (%): C, 56.21; H, 4.71; N, 6.57; Ni, 13.77. FT-IR (cm^{-1}): phenolic υ(OH) 3414, azomethine υ(C=N) 1645, υ(C-N) 1365, phenolic υ(C-O) 1237, υ(H_2O) stretching bands of coordinated water 971 and 807, υ(M-O) stretching bands of coordinated water 560, metal-oxygen bond υ(M-O) 584, metal-nitrogen bond υ(M-N) 466. Molar conductivity(10^{-3} M, DMSO): 45.5 Ω^{-1} cm^2 mol^{-1}. μ_{eff} = 2.76 B.M. λ_{max} (cm^{-1}): 46082 and 41152 (π–π*), 29850 (n–π*).

[Cu(L)(OH$_2$)$_2$].H$_2$O (6)

Yield 64.12 %; black solid, m.p. >300 °C. Anal. Calcd. for Cu($C_{20}H_{20}N_2O_5$) (%): C, 55.62; H, 4.63; N, 6.49; Cu, 14.72. Found (%): C, 55.61; H, 4.62; N, 6.50; Cu, 14.73. FT-IR (cm^{-}

^{1}): phenolic υ(OH) 3436, azomethine υ(C=N) 1615, υ(C-N) 1383, phenolic υ(C-O) 1220, υ(H_2O) stretching bands of coordinated water 953 and 815, υ(M-O) stretching bands of coordinated water 520, metal-oxygen bond υ(M-O) 537, metal-nitrogen bond υ(M-N) 452. Molar conductivity(10^{-3} M, DMSO): 39.7 Ω^{-1} cm^2 mol^{-1}. μ_{eff} = 1.84 B.M. λ_{max} (cm^{-1}) 46082 and 41152 (π–π*), 29850 (n–π*).

[Zn(L)(OH_2)$_2$].H_2O (7)

Yield 61.11 %; yellowish green solid, m.p. 129 °C. Anal. Calcd. for Zn($C_{20}H_{20}N_2O_5$) (%): C, 55.38; H, 4.62; N, 6.46; Zn, 15.09. Found (%): C, 55.40; H, 4.63; N, 6.45; Zn, 15.07. FT-IR (cm^{-1}): phenolic υ(OH) 3424, azomethine υ(C=N) 1651, υ(C-N) 1375, phenolic υ(C-O) 1277, υ(H_2O) stretching bands of coordinated water 962 and 862, υ(M-O) stretching bands of coordinated water 574, metal-oxygen bond υ(M-O) 586, metal-nitrogen bond υ(M-N) 474. Molar conductivity(10^{-3} M, DMSO): 18.1 Ω^{-1} cm^2 $mol^{-1.}$ μ_{eff} = dia.. ^{1}HNMR (300 MHz, DMSO-d_6, δ, ppm): 6.65-7.30 (m, 12H, Ar H), 7.95 (s, 2H, CH=N). λ_{max} (cm^{-1}) 46082 and 40816 (π–π*), 30120 (n–π*).

[Cd(L)(OH_2)$_2$].H_2O (8)

Yield 65.82 %; yellowish green solid, m.p. 140 °C. Anal. Calcd. for Cd($C_{20}H_{20}N_2O_5$) (%): C, 49.96; H, 4.16; N, 5.83; Cd, 23.40. Found (%): C, 49.98; H, 4.17; N, 5.81; Cd, 23.38. FT-IR (cm^{-1}): phenolic υ(OH) 3374, azomethine υ(C=N) 1617, υ(C-N) 1372, phenolic υ(C-O) 1273, υ(H_2O) stretching bands of coordinated water 978 and 862, υ(M-O) stretching bands of coordinated water 573, metal-oxygen bond υ(M-O) 590, metal-nitrogen bond υ(M-N) 460 Molar conductivity(10^{-3} M, DMSO): 7.0 Ω^{-1} cm^2 mol^{-1}. μ_{eff} = dia. λ_{max} (cm^{-1}) 46082 and 40816 (π–π*), 30120 (n–π*).

2.5. Biological Activity

2.5.1. Antimicrobial Activity

Antimicrobial activity of the tested samples was determined using a modified Kirby-Bauer disc diffusion method [31]. 100 µl of the tested bacteria or fungi were grown in 10 ml of fresh media until they reached a count of approximately 108 cells/ml for bacteria and 105 cells/ml for fungi [32]. 100 µl of microbial suspension was spread onto agar plates corresponding

to the broth in which they were maintained. Isolated colonies of each organism that might be playing a pathogenic role should be selected from primary agar plates and tested for susceptibility by disc diffusion method. Of the many media available, NCCLS recommends Mueller-Hinton agar due to: it results in good batch-to-batch reproducibility. Disc diffusion method for filamentous fungi tested by using approved standard method (M38-A) developed [33]. For evaluating the susceptibilities of filamentous fungi to antifungal agent. Disc diffusion method for yeast developed by using approved standard methode (M44-P) [34].

Plates inoculated with Gram (+) bacteria as *Staphylococcus aureus* and *Bacillus subtilis*; Gram (-) bacteria as *Pseudomonas aeruginosa, Salmonella SP.* and *Escherichia coli*, they were incubated at 35-37 ºC for 24-28 hours and yeast fungus as *Aspergillus fumigatus* and *Candida albicans* incubated at 30 ºC for 24-28 hours and, then the diameters of the inhibition zones were measured in millimeters [34]. Standard discs of Ampicillin and Gentamycin (antibacterial agents), and Amphotericin B (antifungal agent) served as positive controls for antimicrobial activity but filter discs impregnated with 10 µl of solvent (distilled water, chloroform, DMSO) were used as a negative control. The agar used is Meuller-Hinton agar that is rigorously tested for composition and pH. Further the depth of the agar in the plate is a factor to be considered in the disc diffusion method. This method is well documented and standard zones of inhibition have been determined for susceptible and resistant values. Blank paper discs (Schleicher and Schuell, spain) with a diameter of 8.0 mm were impregnated with 10 µl of tested concentration of the stock solutions. When a filter paper disc impregnated with a tested chemical is placed on agar, the chemical will diffuse from the disc into the agar. This diffusion will place the chemical in the agar only around the disc. The solubility of the chemical and its molecular size will determine the size of the area of chemical infiltration around the disc. If an organism is placed on the agar, it will not grow in the area around the disc if it is susceptible to the chemical. This area of no growth around the disc is known as zone of inhibition or clear zone. For the disc diffusion, the zone diameters were measured with slipping calipers of the national committee for clinical laboratory standards [35]. Agar based methods such Etest and disc diffusion can be good alternatives because they are simpler and faster than broth-based methods [36].

3. Results and discussion

3.1. Characterization of tetradentate ligand (H_2L)

The parent H_2L is a yellowish green powder, soluble in various solvents. The elemental analyses of the new H_2L (Experimental part) are consistent with the proposed structure as shown in Scheme 1.

The symmetric Schiff base ligand was prepared by condensation an appropriate amount of 2-hydroxybenzaldehyde with *m*-phenylenediamine in 2:1 ratio using ethanol as solvent. The formed new Schiff base ligand was characterized using elemental and spectral analyses.

3.2. Mass Spectrum of tetradentate ligand (H_2L)

Mass spectrum of the ligand gave vital clues for elucidating the structure and to determine the stoichiometry of the compound. The mass spectrum of the ligand shows a well defined molecular ion peak at m/z = 316 corresponding to the $[C_{20}H_{16}N_2O_2]^+$ ion which coincides with the formula weight of the Schiff base.

3.3. FT-IR Spectrum of the ligand (H_2L)

There is a pair of medium intensity bands present at 3200–3400 cm^{-1} in the FT-IR spectrum of *m*-phenylenediamine corresponding to $\upsilon(NH_2)$ stretching vibration. These bands were disappeared in the spectrum of the Schiff base ligand. Also, no strong FT-IR absorption band is observed at 1735 cm^{-1} indicating the absence of υ(C=O) group of 2-hydroxybenzaldehyde. This indicates that the condensation of carbonyl groups of 2-hydroxybenzaldehyde and amino groups of *m*-phenylenediamine has taken place in the reaction [37]. A new band at 1617 cm^{-1} corresponding to azomethine υ(C=N) stretching vibration was recorded due to this condensation reaction confirming the formation of the Schiff base ligand [38].

3.4. ^{1}H NMR Spectrum of the ligand (H_2L)

^{1}H NMR spectrum of ligand at 300 MHz in DMSO-d_6 exhibit a singlet at δ 9.05 ppm (s, 2H) attributed to azomethine (-CH=N-) protons. Other signals are observed in the spectrum of ligand in the range of δ 6.91-8.71 ppm (m, 12H) due to the aromatic rings system protons. The singlet signal at δ 13.00 ppm (s, 2H, OH) is assigned to phenolic protons [39].

3.5. Molecular docking study of the ligand (H_2L)

The purpose of studying molecular docking is to simulate the molecular recognition process by achieving an optimized conformation for the protein and drug with relative orientation between them such that the free energy of the overall system is minimized [1,40-43]. Molecular docking has been studied between ligand (H_2L) and two types of proteins which are receptors of the LYASE / LYASE INHIBITOR Crystal structure of *Escherichia coli* MenB in complex with substrate analogue OSB-NCoA (3T88) and TRANSFERASE Crystal structure of *Staphylococcus aureus* nucleoside diphosphate kinase complexed with ADP (3Q8U). The docking studies show an acceptable interaction between the ligand (H_2L) and the receptor of each protein as showed in Fig. 1. Fig. 2 shows HB plot curves due to the binding of the ligand (H_2L) to the proteins by hydrogen bonding interactions. The calculated binding energy values are tabulated in Table 1. 2D plot and HB plot curves of docking with H_2L ligand are shown in Fig. 3. From Table 1, the value of estimated free energy of binding (kcal/mol) indicated that ligand (H_2L) is higher and stronger inhibitory activity against receptor target. According to the results showed in Table 1, the receptor of *Escherichia coli* (3T88) shows the best interaction than the receptor of *Staphylococcus aureu* (3Q8U) with the ligand (H_2L).

3.6. Compositions and structures of the complexes

The proposed structure in Fig. 4 suggests that the molecular formula of the H_2L is $C_{20}H_{16}N_2O_2$ which upon chelation coordinates with central atom at four coordination sites and with two water molecules (except chromium one water molecule and one chloride atom). All complexes are colored, air stable in the solid state, having high melting points. These complexes are soluble in DMF, DMSO and ethanol. The results of elemental analysis for the complexes were in good agreement with the calculated values showing that the complexes have 1:1 metal–ligand stoichiometric ratio.

3.7. Molar conductance measurements

Molar conductivity ($\Lambda_m\ \Omega^{-1}mol^{-1}\ cm^2$) data was measured using 10^{-3} M solutions of the complexes in DMF or ethanol as solvent at 25°C gave the values (43.1, 33.8, 46.8, 45.5, 39.7, 18.1 and 7 $\Omega^{-1}mol^{-1}\ cm^2$) of the Cr(III), Mn(II), Co(II), Ni(II), Cu(II), Zn(II) and Cd(II)

complexes with Schiff base ligand, respectively. They are considered non-electrolytes due to the absence of any counter ions in their structures [44]. In addition Fe(III) complex has molar conductance value of 63.9 $\Omega^{-1}mol^{-1}$ cm^2, indicating its ionic nature and is considered as 1:1 electrolyte.

3.8. IR spectra analyses

Information about the coordination mode (metal–ligand bonding) of the Schiff bases to metal centers was obtained by recording IR transmission spectra in the regions of 4000-400 cm^{-1} for each new complex and compared the data with free ligand infrared absorptions (Table 2). IR spectra also provide information about the involving of the solution anions to bond formation with transition metal ions. Moreover, the appearance of absorption bands in the region 3500–3200 cm^{-1} is indicative of the presence of water molecules in the structure of the complexes. Table 2 summarizes the main IR bands of the Schiff base ligand and its complexes.

The IR spectrum of the ligand displayed a strong band at 1617 cm^{-1} arises from the azomethine group υ (-CH=N-) stretching frequency [45]. In the FT-IR spectra of the metal complexes the azomethine υ (-CH=N-) band is shifted to higher or lower frequency and appeared at 1615-1651 cm^{-1} [46] indicating coordination through the azomethine-nitrogen with the metal ions. The spectrum of free ligand shows strong bands at 1276 and 1386 cm^{-1}, respectively assigned to υ (C-O) phenolic and υ (C-N) stretching vibrations of the ligand. However, after complexation via oxygen and nitrogen to the metal ion, these bands were observed at the regions of 1220-1284 cm^{-1} and 1365-1383 cm^{-1} for υ (C-O) and υ (C-N), respectively in the complexes. The IR spectrum of the free ligand shows a broad band at 3438 cm^{-1} corresponding to υ (OH) (phenolic). The presence of absorption bands at 3374-3436 cm^{-1} for our complexes indicates the presence of water molecules in those complexes as a coordinated ligand, which was assumed in the elemental analysis [47]. The new bands observed for the complexes between 537–590 cm^{-1} and 450–474 cm^{-1} were metal sensitive and are assigned to υ (M–O) and υ (M–N) [1], respectively.

The presence of coordinated water is further confirmed by the appearance of non-ligand bands in the region of 807-872 cm^{-1} and 937-978 cm^{-1} assignable to the rocking mode of coordinated water [48]. The υ(M-O) stretching vibrations of coordinated water attachment to

metal ions are found at 520-574 cm^{-1} for the complexes. The presence of coordinated water in all these complexes is proved by thermal analysis. The presence of lattice water in the complexes is also confirmed by TG and DTG analysis.

Thus, the IR data suggest that the Schiff base is a binegative tetradentate ligand bound to the metal ions through the two deprotonated phenolic oxygen atoms and azomethine nitrogens with ONNO donor atoms.

3.9. ^{1}H NMR spectrum of Zn(II) complex (7)

A comparison of the ^{1}H NMR spectrum of the complex (**7**) with parent ligand (Table 3) shows that the OH phenolic signal, occurring in the spectrum of the ligand at δ 13.00 ppm, completely disappears in the spectrum of its metal complex (**7**), indicating that the two OH protons are removed by coordination with the metal ions. In addition, the imino protons bands are significantly shifted in the complex and appeared at δ 7.95 ppm, due to coordination through the azomethine nitrogen atoms of the ligand. Aromatic protons are shifted in the spectrum of the complex and appeared at δ 6.65-7.30 ppm [49-51]. From ^{1}H NMR, it is concluded that the ligand is binegative tetradentate ligand coordinated to the metal ion through the two nitrogen atoms of azomethine and the two deprotonated phenolic oxygen.

3.10. Mass spectrum of complex

The mass spectrum of Cd(II) complex shows a molecular ion peak at m/z = 480 corresponding to the formula $[Cd(L)(H_2O)_2].H_2O$ (Calcd. 480.411 g/mol). The proposed formula of the complex was confirmed by the observed peak at 316 corresponding to the ligand moiety [($C_{20}H_{16}N_2O_2$) atomic mass 316 amu]. These data confirmed the stoichiometry of the complex as being of [ML] type.

3.11. UV–Visible spectra

1 x 10^{-4} M solutions of the prepared ligand and its complexes were recorded over the wavelength range 200-700 nm in ethanol solvent. The UV–Vis spectrum of the ligand exhibits a band at 44843 cm^{-1} attributed to $\pi \rightarrow \pi^*$ transition within the free ligand [1,52]. Another absorption band observed at 26809 cm^{-1} for the ligand due to $n \rightarrow \pi^*$ transition between lone-

pair electrons of the p orbital of the N atom in the azomethine group and the O atom of the hydroxyl group [22].

3.12. Electronic spectra and magnetic moment measurements

There are three absorption bands at 15,565, 21,861, and 27,700 cm^{-1}in the electronic spectrum of the Cr(III) complex shows. The three spin-allowed transitions for Cr(III) in an octahedral field are as follows: $^4A_{2g}(F) \rightarrow {}^4T_{2g}(F)$, $^4A_{2g}(F) \rightarrow {}^4T_{1g}(F)$, and $^4A_{2g}(F) \rightarrow {}^4T_{1g}(P)$ transitions, respectively. The magnetic moment value of Cr(III) complex is found to be 3.58 B.M. which is in agreement with the presence of three unpaired electrons [53].

The diffused reflectance spectrum of Mn(II) complex exhibits three bands at 27,124, 19,347 and 15,436 cm^{-1} which may be assigned to $^4T_{1g} \rightarrow {}^6A_{1g}$, $^4T_{2g}(G) \rightarrow {}^6A_{1g}$ and $^4T_{1g}(D) \rightarrow {}^6A_{1g}$ transitions, respectively, h suggesting the octahedral geometry [54,55]. The magnetic moment measurement of the Mn(II) complex (5.43 B.M.) lies in the range of octahedral geometry [28,56] which due to the two coordinated water molecules.

From the diffused reflectance spectrum, it is observed that, the Fe(III) chelate exhibits a band at 21,453 cm^{-1}, attributed to the $^6A_{1g} \rightarrow T_{2g}(G)$ transition in octahedral geometry [57]. The $^6A_{1g} \rightarrow {}^5T_{1g}$ transition appears to be split into two bands at 15,426 and 13,362 cm^{-1}. The Fe(III) complex is found to have magnetic moment value of 5.17 B.M., suggesting octahedral geometry involving sp^3d^2 hybridization in Fe(III) ion [58].

The electronic spectrum of Co(II) complex shows bands at 13,223, 15,193 and 22,153 cm^{-1} which are attributed to the electronic transition $^4T_{1g}(F) \rightarrow {}^4T_{2g}(F)$, $^4T_{1g}(F) \rightarrow {}^4A_{2g}(F)$ and $^4T_{1g}(F) \rightarrow {}^4T_{1g}(P)$, respectively, indicating that there is an octahedral geometry around Co(II) ion [59,60]. The magnetic susceptibility measurement lie at 5.18 B.M. is an indicative of octahedral geometry.

The ligand field parameters B (interelectronic repulsion of the d-electrons in complexes) (155 cm^{-1}), β (nephelauxetic effect) (0.16) and 10Dq (1970 cm^{-1}) are calculate [1,28]. These results show that the B of the d-electrons is less than that in the free ion. The β value is related directly to covalence. The reduction of B on complex formation is caused by delocalization of

the d-electron cloud on the ligand, which is in turn caused by the formation of covalent bond. The data show the Co(II) complex has covalent character [28,23].

Also, the Ni(II) complex exhibits four electronic spectral bands at 26,146, 20,498, 14,593 and 13,245 cm^{-1} which may be assigned to charge transfer (LMCT), $^3A_{2g}(F) \rightarrow {}^3T_{2g}(F)$, $^3A_{2g}(F) \rightarrow {}^3T_{1g}(F)$ and $^3A_{2g}(F) \rightarrow {}^3T_{1g}(P)$ transitions, respectively. The position of these bands suggested an octahedral geometry around the Ni(II) ion [61–66]. This geometry is further supported by its magnetic susceptibility value (2.76 BM). The values of 10Dq and B are 1459 and 191 cm^{-1}, respectively, and β is 0.18. These results show that the interelectronic repulsion of the d-electron in a complex is less than that in free ion.

The reflectance spectrum of the Cu(II) chelate shows a broad band at 15,463 and 20,498 cm^{-1}. The ^2E_g and $^2T_{2g}$ states of the octahedral Cu(II) ion (d^9) split under the influence of the tetragonal distortion and the distortion can be such as to cause the three transitions $^2B_{1g} \rightarrow {}^2B_{2g}$, $^2B_{1g} \rightarrow {}^2E_g$ and $^2B_{1g} \rightarrow {}^2A_{1g}$ to remain unresolved in the spectrum [53,67]. This assignment is in agreement with the general observation that Cu(II) d–d transitions are normally close in energy [53]. The magnetic moment of 1.84 B.M. falls within the range normally observed for octahedral Cu(II) complex [53, 67]. A moderately intense peak observed in the range 25,664 cm^{-1} is due to ligand to metal charge transfer transition [53].

According to the empirical formulae of the Zn(II) and Cd(II) complexes, an octahedral geometry is proposed for these complexes.

3.13. Theoretical study of the ligand (H_2L) and its metal complexes

The electronic properties and geometrical structures of the ligand (H_2L) and its metal complexes were calculated by optimizing their bond lengths and bond angles. The optimized structures of the ligand (H_2L) and its metal complexes are presented in Fig. 5. Bond lengths and bond angles of the ligand (H_2L) and its metal complexes are listed in Tables S1-S8. The HOMO and LUMO for tetradentate ligand (H_2L) and its metal complexes are shown in Fig. 6. Quantum chemical parameters of the ligand (H_2L) and its metal complexes are obtained from calculations such as energies of the highest occupied molecular orbital (E_{HOMO}) and the lowest unoccupied molecular orbital (E_{LUMO}) as listed in Table 4. Additional parameters such as HOMO–LUMO energy gap, ΔE, additional electronic charge, ΔN_{max}, global softness, *S*, chemical potentials, Pi,

absolute hardness, η, absolute softness, σ, global electrophilicity, ω and absolute electronegativities, χ, are calculated using the equations [29,42,68] and listed in Table 4.

The values of ΔE for the ligand (H_2L) and its metal complexes (1, 2, 4-8) were found to be 3.063, 1.039, 0.419, 2.864, 0.631, 2.688, 2.575 and 1.920 eV, respectively.

3.14. Thermal analyses studies

The thermal behavior of ligand and its metal complexes has been characterized (see Supplementary data) on the basis of a thermogravimetric (TG) method to check the presence of water molecules in the coordination sphere of metal complexes. The thermal analysis gave useful data for the thermal stability of the metal complexes. The TG and DTG were recorded within the temperature range from 30 to 1000 °C (Table 5).

In hydrated complexes, water could be held by bonding to the metal ion or it may be held as lattice or crystal water. In some of the present complexes, the DTG curve showed that dehydration occurred at relatively high temperature outside the range for lattice water. Hence, the water molecules could be considered to be involved in bonding due to the high temperature associated with this step [69].

The thermal decomposition process of H_2L Schiff base ligand with the molecular formula [$C_{20}H_{16}N_2O_2$] involves four decomposition steps. Decomposition of the ligand started at 45°C and finished at 1000°C with four stages. The first stage of decomposition involves the loss of $C_4H_6O_2$ molecule in 45-305°C temperature range, and is accompanied by a weight loss of 27.21 % (calcd. = 27.22 %). The second stage of decomposition occurs in the 305-535°C temperature range, corresponding to the loss of $C_4H_4N_2$ molecule, and is accompanied by a weight loss of 25.30 % (calcd. = 25.31 %). The third stage involves the removal of C_6H_4 molecule in the temperature range from 535-700°C, and is accompanied by a weight loss of 24.03 % (calcd. = 24.05 %). While the fourth stage involves the removal of C_6H_2 molecule in the temperature range from 700-1000°C, and is accompanied by a weight loss of 23.41 % (calcd. = 23.42 %). The total weight loss amounts to 99.95 % (calcd 100 %).

The thermal decomposition of the complex (**1**) occurs in the temperature interval of 25–1000°C. TG curve of the [Cr(L)Cl(H_2O)].H_2O complex shows five steps of decomposition. The

first and second stages of decomposition occur in the 25-285°C temperature range, corresponding to the loss of HCl, N_2 and $2H_2O$ molecules, and are accompanied by a weight loss of 22.74 % (calcd 22.96 %). While the third stage involves the removal of $C_4H_3O_{0.5}$ molecule in the 285–415°C temperature range, and is accompanied by a weight loss of 13.25 % (calcd 13.49 %). The next weight loss of 14.62 % (calcd. 14.63 %) at 415–590°C is attributed to the loss of C_5H_4 fragment. Finally, the remaining of the ligand is lost with a weight loss of 23.21% (calc. 23.32 %) at 590–1000°C due to the loss of C_8H_6 organic moiety, leaving the carbon and chromium oxide remained as residues. The total weight loss amounts to 73.82 % (calcd 74.4 %).

The TGA curve of complex (**2**) showed that the thermal decomposition takes place at a temperature range 10-1000°C. The first and second decomposition steps occurred at 10-135°C due to weight loss of 12.26 % (Calcd. 12.77 %) corresponded to the elimination of three H_2O molecules. The third stage of decomposition was due to the loss of CH_4 molecule at a temperature range 135-180°C and showed an estimated mass loss of 3.73 % (Calcd. 3.78 %), while the fourth stage of decomposition at 180-245°C was referred to the loss of 6.02 % (Calcd. 6.15 %) corresponding to the elimination of C_2H_2 organic molecule. The fifth and sixth decomposition steps occurred at 245-670°C due to weight loss of 21.72 % (Calcd. 21.75 %) corresponding to the elimination of C_5H_4 and N_2 molecules. The last step was referred to the loss of 15.83 % (Calcd. 16.08 %) due to the release of C_4H_4O ligand molecule to give finally MnO contaminated with carbonas residue. The total weight loss amounts to 59.56 % (Calcd. 60.53 %).

The complex (**3**) was thermally decomposed in three successive decomposition steps. The first step with estimated mass loss of 22.28 % (calculated mass loss = 22.30 %) within the temperature range 35–295°C may be attributed to the loss of $2.5H_2O$, HCl and NH_3 molecules. The second step occurred within the temperature range 295-680°C with an estimated mass loss 25.53 % (calculated mass loss = 25.60 %), which correspond to the loss of C_8NH_3 fragment. The final step occurred within the temperature range 680-1000°C with estimated mass loss 6.72 % (calculated mass loss = 6.79 %), which correspond to the loss of C_2H_6 fragment. The overall weight loss amounted to 54.53 % (calculated mass loss = 54.69 %). The TG thermogram shows that the complex gradually decomposed at 35-1000°C, ended with formation of contaminated metal oxide ($½Fe_2O_3$) with carbon and they are left as a residue.

The thermal analysis of the complex (**4**) suggested three water molecules per complex compound. Two of them are coordinated with the metal ion, and the third one is water from hydration. Thermal analysis of the complex indicated loss of weight in the following four steps: the first step corresponds to a small weight loss in the range of 10-95°C due to loss of $1.5H_2O$ molecule. The weight loss amounted to 6.32 % (calculated mass loss = 6.33 %). The second step corresponds to weight loss in the range of 95-375°C attributable to the loss of $1.5H_2O$ and C_4H_2 molecules. The weight loss amounted to 17.71 % (calculated mass loss = 18.04 %). The third step corresponds to gradual weight loss in the range of 375-630°C, which can be assigned to the loss of $C_4H_6N_2$ organic moiety. The weight loss amounted to 19.13 % (calculated mass loss = 19.20 %). The last step represents gradual weight loss from 630-1000°C, which can be assigned to complete decomposition of the ligand moiety with a loss of C_3H_6O molecule with an estimated mass loss of 13.39 % (calculated mass loss = 13.59 %). leaving the metal ion CoO contaminated with carbon as a residue. The overall weight loss amounted to 56.55 % (calcd. = 57.16 %).

TG curve of the complex (**5**) indicates that the complex is thermally decomposed in four steps in the temperature range from 15 to 1000°C. The first and second stages of decomposition occur in the 15-440°C temperature range, corresponding to the loss of C_8H_2 and $3H_2O$ molecules of uncoordinated and coordinated water, and are accompanied by a weight loss of 35.10 % (Calcd. 35.63 %). In the third stage of decomposition, the TG curve for the complex shows a mass reduction in the temperature range 440-565°C which is due to weight loss of 7.43 % (Calcd. 7.50 %) corresponding to the elimination of CH_3OH organic molecule. The last step of the thermal decomposition, which occurs in the range 565-1000°C, is assigned to the loss of CH_4 and N_2H_4 organic molecules (observed 10.80 %) (Calcd. 11.25 %) leaving NiO contaminated with carbon as residue. The overall weight loss amounted to 53.33 % (calcd. = 54.38 %).

The thermal decomposition process of the copper complex (**6**) occurs in four steps. In the TG graph of the complex, the weight loss of 4.44 % (calc. 4.63 %) at 10-135°C corresponds to the departure of the lattice water and the free hydrogen molecule. In the second step, the weight loss of 18.75 % (calc. 18.77 %) at 135-410°C is associated with the separation of the two coordinated water molecules and the organic moiety C_2H_7N. While the third and fourth stages involve the removal of C_5H_5NO molecule in the 410-1000°C temperature range, and is

accompanied by a weight loss of 22.01 % (calcd 22.02 %). The overall weight loss amounted to 45.20 % (calcd. = 45.42 %).

The complex (**7**) (gave decomposition pattern started at 10°C and finished at 1000°C with three stages. The first stage was one step within the temperature range of 10-140°C, representing the loss of H_2O (hydrated) with a found mass loss of 4.13 % (calcd. = 4.15 %). The second stage was also one step representing the loss of $2H_2O$ and C_2NH_3 molecules with a mass loss of 17.75 % (calcd. = 17.77 %) within the temperature range 140-375°C. The final stage was also one step representing the loss of $C_8H_{11}NO$ molecule with a mass loss of 31.59 % (calcd. 31.61 %) within the temperature range 375-1000°C. At the end of the thermogram, the metal oxide ZnO was the residue, which was contaminated with carbon. The overall weight loss amounted to 53.47 % (calcd. = 53.53 %).

The thermal decomposition process of the complex (**8**) occurs in three steps. In the TG graph of the complex, the weight loss of 5.59 % (calcd. 5.62 %) at 10-225°C at the first step corresponds to the departure of $1.5H_2O$ molecules. The weight loss of 13.92 % (calcd. 13.95 %) at the second step at 225-485°C is associated with the separation of $1.5H_2O$ and C_3H_4 molecules, while the last step with a weight loss of 53.35 % (calc. 53.70 %) at 485-1000°C is attributed to loss of $C_{14}H_6N_2$ and C_3H_4O organic moieties. The residual weight of 27.14 % (calc. 26.73 %) corresponds to cadmium oxide, CdO molecule. The overall weight loss amounted to 72.86 % (calcd. = 73.27 %).

3.15. Scanning Electron Microscope (SEM) analysis

The SEM images of free ligand H_2L and its Cd(II) and Co(II) complexes showed different morphologies as shown in Fig. 7. The SEM image of ligand seemed as irregularly large-sized sheets with average size 88 nm. The SEM image of Co(II) complex seemed as glass sheets crystals with average size 61 nm. The SEM image of Cd(II) complex seemed as irregularly perpendicular walls with some rods with average size 49 nm.

3.16. Structure interpretation

From the IR spectra, it is concluded that H_2L behaves as bi-negative tetradentate ligand coordinated to the metal ions via the two deprotonated phenolic oxygen and two azomethine nitrogen atoms. The ^1H NMR spectra of the free ligand and the diamagnetic complex (**7**) showed

that the deprotonated OH groups and azomethine nitrogen atoms of H_2L ligand participate in chelation. The analytical data were in good agreement with the proposed molecular formula of the ligand and the complexes. From conductance measurements, the complexes are non-electrolytes except Fe(III) complex, it is found to be 1:1 electrolyte. The general formulae of the complexes are suggested as the following:

$[Cr(L)(H_2O)Cl]\ H_2O$, $[M(L)(H_2O)_2]\ H_2O$, (M = Mn(II), Co(II), Ni(II), Cu(II), Zn(II) and Cd(II)) and $[Fe(L)(H_2O)_2]\ Cl$.

On the basis of the above observations and from the magnetic and solid reflectance measurements, octahedral geometry is suggested for the investigated complexes. The structures of complexes are shown in Fig. 4.

3.17. Biological activity

The biological activity of the ligand and its metal complexes (Table 6) were studied in vitro against two fungi species *Aspergillus fumigates* and *Candida albicans,* two gram positive bacteria *Staphylococcus aureus* and *Bacillis subtilis* and three gram negative bacteria *Salmonella SP., Escherichia coli* and *Pseudomonas aeruginosa* by using diffusion technique. The inhibition zone ion was measured directly from the scale and compared with DMSO as blank and standard compounds. Ampicillin and Gentamycin illin were used as reference compounds for antibacterial activity and Amphotericin B was used as a reference compound for antifungal activity.

The increased activity of the metal chelates can be explained on the basis of chelation theory [70, 71]. According to the concept of cell permeability, the lipid membrane surrounds the cell favours the passage of only lipid-soluble materials due to the fact that liposolubility is considered to be an important factor that controls antimicrobial activity. On chelation, the polarity of the metal ion will be reduced to a greater extent due to the partial sharing of positive charge of metal ions with donor groups and the overlap of the ligand orbital. Furthermore, it increases the delocalization of the electrons over the whole chelate ring and enhances the lipophilicity of the complex. This increased lipophilicity enhances the penetration of the complexes into the lipid membrane and thus blocks the metal binding sites on enzymes of microorganisms. These metal complexes also disturb the respiration process of the cell and thus

block the synthesis of proteins, which restricts further growth of the organism. The variation in the activity of different complexes against different organisms depends either on the impermeability of the microbe's cells or difference in the microbe's ribosomes.

The best antimicrobial activities of the ligand (H_2L) agreed its predicted best inhibitory effect to receptors of *Escherichia coli* (3T88) and *Staphylococcus aureus* (3Q8U). These results are found to be in good agreement with the similar results were obtained recently [72].

The bacterial growth inhibitory capacity of the complexes was compared to that of the ligand. It was found that Co(II) and Cd(II) complexes showed the most antibacterial activities against *Staphylococcus aureus*, *Bacillus Subtilis*, *Escherichia coli* and *Pseudomonas aeruginosa* (Fig. 8), while Mn(II) complex showed the lowest activity against these microorganisms. The high activity of the parent ligand and its Co(II) and Cd(II) complexes may be related by their nano sized structures that is proven depending on SEM imaging. All complexes showed antifungal activities higher than the ligand against *Aspergillus fumigates* and *Candida albicans* organisms except for Fe(III) complex which have lower antifungal activity against *Candida albicans* than the ligand. Of all complexes, Cd(II) showed the highest antifungal activitiy against *Candida albicans* and *Aspergillus fumigates*.

4. Conclusion

The data of Schiff base ligand (H_2L: 2,2'-((1E,1'E)-(1,3 phenylene bis (azanylylidene)) bis (methanylylidene))diphenol) derived from *m*-phenylenediamine and 2-hydroxybenzaldehyde showed that the chelation occurs through the deprotonated phenolic oxygen and azomethine nitrogen atoms of the ligand and the complexes have composition of ML type. The nature of bonding and the stereochemistry of the complexes were deduced from elemental analysis, infrared spectra, magnetic moments and conductivity measurements and thermal analysis. From magnetic moment and electronic spectral studies, all complexes showed an octahedral geometry around the transition metal ions. The presence of coordinated water molecules in all the complexes has been further confirmed from thermal analysis. The antibacterial studies of the prepared compounds screened against pathogenic bacteria proved that these compounds exhibited selective antibacterial activity. The complexes are more active as compared to their free ligand. This implies an increase in the antibacterial activity with coordination.

References

[1] Sh.M. Morgan, A.Z. El-Sonbati, H.R. Eissa, J. Mol. Liq. 240 (2017) 752–776.

[2] I.A. Koval, M. Huisman, A.F. Stassen, P. Gamez, M. Lutz, A.L. Spok, D. Pursche, B. Krebs, I. Reedijk, Inorg. Chem. Acta 357 (2004) 294.

[3] Z.Y. Tian, L.N. Song, Y. Zhao, F.L. Zang, Z.H. Zhao, N.H. Chen, X.J. Xu J, C.J. Wang, Molecules 20 (2015) 16491–16523.

[4] J. Nandre, S. Patil, P. Patil P, S. Sahoo, C.Redshaw, P. Mahulikar, U. Patil, J. Fluoresc, 24 (2014) 1563–1570.

[5] S. Zhu S, J. Zhang, J. Janjanam, G. Vegesna, F.T. Luo, A. Tiwari, H. Liu, J. Mater. Chem. B 1 (2013) 1722–1728.

[6] A. Rezaeifard, M. Jafarpour, M.A. Nasseri, R. Haddad, Helvetica Chimica Acta **93** (2010) 711.

[7] H.L. Singh, M. Sharma, M.K. Gupta, A.K. Varshney, Synth. React. Inorg. Met-Org. Chem. **30** (2000) 445.

[8] L.Z. Li, Z.H. Guo, Q.F. Zhang, T. Xu, D.Q. Wang, Inorg. Chem. Commun. **13** (2010) 1166.

[9] R. Pal, V. Kumar, A.K. Gupta, V. Beniwal, J. Med. Chem. Res., 23 (2014) 3327–3335.

[10] W.H. Mahmoud, R.G. Deghadi, G.G. Mohamed, Appl. Organomet. Chem. 30 (2016) 221–230.

[11] R. Eglof, P. Piotr, B. Bogumil, B.Franz, Curr. Org. Chem. 13(2009) 241–249.

[12] S.L. Kessel, R.M. Emberson, P.G. Debunner, D.N. Hendrickson, Inorg. Chem. 19 (1980) 1170– 1178.

[13] X. Wang, D. Shi, Y. Xu, S. Yu, F. Zhao, Y. Wang, L. Hu, J. Tian, X. Yu, L. Pu, Tetrahedron Lett., 59 (2018) 2332-2334.

[14] Z. Saedi, E. Hoveizi, M. Roushani, S. Massahi, M. Hadian, K. Salehi. .J. Mol. Stru., 1176 (2019) 207-216.

[15] L. Touafri, A. Hellal, S. Chafaa, A. Khelifa, A. Kadri, J. Mol. Stru., 1149 (2017) 750-760.

[16] H. Abou-Yousef, T A. Khattab, Y. A. Youssef, N. Al-Balakocy, S. Kamel. Talanta 170 (2017) 137-145.

[17] J. Long, I. V. Basalov, N. V. Forosenko, K. A. Lyssenko, E. Mamontova, A. V. Cherkasov, M. Damjanović et al, Chemistry-A European Journal (2018)

[18] A. Saini, C. W. Christenson, T. A. Khattab, R. Wang, R. J. Twieg, K. D. Singer, J. Appl. Phys., 121 (2017) 043101.

[19] B. O. Okesola, D. K. Smith, Chem. Soc. Rev., 4515 (2016) 4226-4251.

[20] T. A. Khattab, H. E. Gaffer, Color. Techn., 132 (2016) 460-465.

[21] T. A. Khatam, J. Mol. Stru., 1169 (2018) 96-102.

[22] R. Sarin, K. N. Mushi, J. Inorg. Nucl. Chem., 34 (1972)581.

[23] Sh.M. Morgan, A.Z. El-Sonbati, M.A. El-Mogazy, Appl. Organometal. Chem., 32 (2018) e4264.

[24] A.Z. El-Sonbati, M.A. Diab, Sh.M. Morgan, A.M. Eldesoky, M.Z. Balboula, Appl. Organometal. Chem. 32 (2018) e4207.

[25] A.Z. El-Sonbati, M.A. Diab, Sh.M. Morgan, H.A. Seyam, J. Mole. Struct. 1154 (2018) 354–365.

[26] A.Z. El-Sonbati, M.A. Diab, Sh.M. Morgan , M.A. El-Mogazy, Appl. Organometal. Chem. 32 (2018) e4530.

[27] A.Z. El-Sonbati, M.A. Diab, Sh.M. Morgan, M.Z. Balboula, Appl. Organometal. Chem. 32 (2018) e4059.

[28] Sh.M. Morgan, M.A. Diab, A.Z. El-Sonbati, Appl. Organometal. Chem. 32 (2018) e4281.

[29] Sh.M. Morgan, M.A. Diab, A.Z. El-Sonbati, Appl. Organometal. Chem. 32 (2018) e4305.

[30] Sh.M. Morgan, M.A. Diab, A.Z. El-Sonbati, Appl. Organometal. Chem. 32 (2018) e4504.

[31] A.W. Bauer, W.M. Kirby, C. Sherris, M. Turck, Am. J. Clin. Path., 45, 493, 1966.

[32] M.A. Pfaller, L. Burmeister, M.A. Bartlett, M.G. Rinaldi, J. Clin. Microbiol., 26, (1988)1437.

[33] National Committee for Vlinical Laboratory Standards. Reference method for broth dilution antifungal susceptibilty testing of conidium-forming filamentous: proposed standard M38-A. Wayne, PA, USA, 2002.

[34] National Committee for Vlinical Laboratory Standards. Method for antifungal disc diffusion susceptibility testing of yeast: proposed guideline M44-P, Wayne, PA, USA, 2003.

[35] L.D. Liebowitz, H.R. Ashbee, E.G.V. Evans, Y. Chong, N. Mallatova, M. Zaidi, D. Gibbs, Global Surbeillance Group. Diagn. Microbiol. Infect. Dis., 4 (2001) 27.

[36] M.J. Matar, L.O. Zeichner, V.L. Paetznick, J.R. Rodriguez, E. Chen, J.H. Rex. Agents Chemother., 47 (2003)1647.

[37] D. P. Singh, V. Malik, K. Kumar, C. Sharma, K. R. Aneja, Spectrochim. Acta A, 76(2010) 45–9.

[38] B. Shafaatian, Z. Ozbakzaei, B. Notash, S. A. Rezvani, Spectrochim. Acta A 5 (2014) 248–255.

[39] N.A. El-Ghamaz, M.A. Diab, A.Z. El-Sonbati, Sh.M. Morgan, O.L. Salem, Chem. Pap. 71 (2017) 2417–2433.

[40] G.G. Mohamed, A.A. El-Sherif, M.A. Saad, S.E.A. El-Sawy, Sh.M. Morgan, J. Mol. Liq. 223 (2016) 1311–1332.

[41] M.A. Diab, A.Z. El-Sonbati, Sh.M. Morgan, M. A. El-Mogazy, *Appl. Organometal. Chem.* 32 (2018) e4378.

[42] A.Z. El-Sonbati, M.A. Diab, Sh.M. Morgan, J. Mol. Liq. 225 (2017) 195–206.

[43] H.M. Refaat, H.A. El-Badway, Sh.M. Morgan, J. Mol. Liq. 220 (2016) 802–812.

[44] E. Tas, M. Aslanoglu, A. Kilic, O. Kaplan, H. Temel, J. Chem. Res. (S) 4 (2006) 242-245.

[45] M.M. Abd-Elzaher, J. Chin. Chem. Soc. 48 (2001) 153.

[46] S. Carla, F. Cristina, C. de Baltazar, Molecules 8 (2003) 894.

[47] H.N. Aliyu, I. Ado, Bayero J. Pure Appl. Sci. 3 (2010) 245–249.

[48] V. Haribabu, P.V. Anantha Lakshmi, V. Jayatyaga Raju, Int. J. Chem. Tech. Res., 5 (2013) 1512–1518.

[49] A.Z. El-Sonbati, A.A.M. Belal, M.S. El-Gharib, Sh.M. Morgan, Spectrochim. Acta A 95 (2012) 627–636.

[50] A.Z. El-Sonbati, M.A. Diab, A.A.M. Belal, Sh.M. Morgan, Spectrochim. Acta A,

99 (2012) 353-360.

[51] M.I. Abou-Dobara, A.Z. El-Sonbati, Sh.M. Morgan, World J. Microbiol.

Biotechnol., 29 (2013) 119 -126.

[52] N.A. El-Ghamaz, A.Z. El-Sonbati, Sh.M. Morgan, J. Mol. Struct., 1027 (2012) 92-98.

[53] F.A. Cotton, G. Wilkinson, C.A. Murillo, M. Bochmann, Advances in Schiff base chemistry, 6^{th} Ed. Wiley, New York (1999).

[54] D.N. Sathyanarayana, Electronic Absorption Spectroscopy and Related Techniques, Orient Longman Limited; Universities Press (India) Limited, 2001.

[55] G.G. Mohamed, H.F. Abd El-Halim, M.M.I. El-Dessouky, W.H. Mahmoud. J. Mol. Str., 111 (2011) 29–38.

[56] W.M.I. Hassan, M.A. Badawy, G.G. Mohamed, H. Moustafa, S. Elramly, Spectrochim. Acta A 111 (2013) 169–177.

[57] G.G. Mohamed, N.E.A. El-Gamel, Spectrochim. Acta A, 60 (2004) 3141–3154.

[58] M. Sakai, A. Hara, A. Anjo, M. Nakamura, J. Pharm. Biomed. Anal. 18 (1999) 1057–1067.

[59] Sh.M. Morgan, N.A. El-Ghamaz, M.A. Diab, J. Mol. Struct. 1160 (2018) 227.

[60] H.F. Abd El-halim, M.M. Omar, G.G. Mohamed, Spectrochim. Acta A 78 (2011) 36-44.

[61] S. Seth, K.K. Aravindakshan, Spectrochim. Acta A 112 (2013) 276–279.

[62] W.M.I. Hassan, M.A. Badawy, G.G. Mohamed, H. Moustafa, S. Elramly, Spectrochim. Acta A 111 (2013) 169–177.

[63] M.M. Al-Ne'aimi, M.M. Al-Khuder, Spectrochim. Acta A 105 (2013) 365–373.

[64] Madiha.H. Soliman, Gehad.G. Mohamed, Spectrochim. Acta A 107 (2013) 8–15.

[65] H.F. Abd El-Halim, G.G. Mohamed, M.M.I. El-Dessouky, W.H. Mahmoud, J. Pharm. Res., 5 (2012) 5084–5092.

[66] Gehad G. Mohamed, M.M. Omar, Amr A. Ibrahim, Eur. J. Med. Chem. 44 (2009) 4801–4812.

[67] G.G. Mohamed, F.A. Nour EL-Dien, S.M. Khalil, A.S. Mohammad, J. Coord. Chem. 62 (2009) 645–654.

[68] A.M. Eldesoky, M.A. El-Bindary, A.Z. El-Sonbati, Sh.M. Morgan, J. Mater. Environ. Sci. 6 (2015) 2260.

[69] V. Uivarosi, M. Badea, V. Aldea, L. Chirigiu, R. Olar, J. Therm. Anal. Calorim. 111, 1177–1182 (2013)

[70] D.A. Chowdhury, M.N. Uddin, N. Lucky, Bull. Pure Appl. Sci. 22 (1) (2003) 39–45.

[71] M.N. Uddin, D.A. Chowdhury, M.T. Islam, F. Hoque, Orbital Electron. J. Chem. 4 (4) (2012) 273–287.

[72] M. I. Abou-Dobara, N.F. Omar, M.A. Diab, A.Z. El-Sonbati, Sh.M. Morgan, M.A. El-Mogazy, J. Cell. Biochem. 120 (2019) 1667–1678.

Table 1. Energy values obtained in docking calculations of the ligand (H_2L) with receptors of *Escherichia coli* (3T88) and *Staphylococcus aureu* (3Q8U).

Receptors	Estimated free energy of binding (kcal/mol)	Estimated inhibition constant (K_i) (µM)	vdW+ bond+ desolv energy (kcal/mol)	Electrostatic Energy (kcal/mol)	Total intercooled Energy (kcal/mol)	Interact surface
3T88	-6.44	18.99	-8.18	-0.08	-8.26	808.28
3Q8U	-5.78 kcal/mol	58.39 uM	-7.30 kcal/mol	-0.12 kcal/mol	-7.41 kcal/mol	870.03

Table 2. IR spectra (4000-400 cm^{-1}) of H_2L ligand and its metal complexes[a]

H_2L	**1**	**2**	**3**	**4**	**5**	**6**	**7**	**8**	Assignment
3438br	3319	3426br	3429br	3428br	3414br	3436br	3424br	3374br	OH stretching
1617sh	1645sh	1647sh	1640sh	1646sh	1645sh	1615sh	1651sh	1617sh	CH=N stretching
1386sh	1378sh	1378sh	1371sh	1382sh	1365sh	1383sh	1375sh	1372sh	C-N stretching
1276sh	1275sh	1275sh	1284sh	1238sh	1237sh	1220sh	1277sh	1273sh	C-O phenolic
-----	896, 932sh	869, 960sh	872, 958sh	853, 937s	807, 971sh	815, 953s	862, 962sh	862, 978sh	H_2O stretch of coordinated water
-----	543s	543s	580s	579s	584sh	537s	586sh	590sh	M-O
-----	535s	530s	570s	538s	560s	520s	574s	573s	M-O stretching of coordinated water
-----	479w	450w	455w	459s	466sh	452w	474sh	460s	M-N

[a]Numbers are given in Experimental part.

sh = sharp, br = broad, s = small, w = weak, m = medium

Table 3. ^{1}H NMR spectral data of H_2L ligand and complex 7.

Compound[a]	Chemical shift, (δ) ppm	Assignment
H_2L	13.00	(s, 2H,OH)
	9.05	(s, 2H, CH=N)
	6.91-8.71	(m, 12H, benzene rings of H_2L)
Complex 7	disappeared	(s, 2H,OH)
	7.95	(s, 2H, CH=N)
	6.65-7.30	(m, 12H, benzene rings of H_2L)

[a]Numbers are given in Experimental part.

Table 4. The calculated quantum chemical parameters of the ligand (H_2L) and its metal complexes

Compound[a]	E_{HOMO} **(eV)**	E_{LUMO} **(eV)**	**ΔE (eV)**	**χ (eV)**	**η (eV)**	**σ $(eV)^{-1}$**	**Pi (eV)**	**S $(eV)^{-1}$**	**ω (eV)**	ΔN_{max}
H_2L	-7.555	-4.492	3.063	6.024	1.532	0.6529	-6.024	0.3265	11.8454	3.9331
1	-10.435	-9.396	1.039	9.916	0.519	1.9249	-9.916	0.9625	94.6267	19.0866
2	-9.602	-9.183	0.419	9.393	0.209	4.7733	-9.393	2.3866	210.5467	44.8329
4	-5.749	-2.885	2.864	4.317	1.432	0.6983	-4.317	0.3492	6.5072	3.0147
5	-8.802	-8.171	0.631	8.487	0.316	3.1696	-8.487	1.5848	114.1374	26.8986
6	-6.787	-4.099	2.688	5.443	1.344	0.7440	-5.443	0.3720	11.0217	4.0499
7	-7.079	-4.504	2.575	5.792	1.288	0.7767	-5.792	0.3883	13.0258	4.4983
8	-6.889	-4.969	1.920	5.929	0.960	1.0417	-5.929	0.5208	18.3089	6.1760

[a]Numbers are given in Experimental part.

Table 5. Thermoanalytical results (TG) of H_2L ligand and its complexes.

Complex[a]	TG range (°C)	DTG_{max} (°C)	n*	Mass loss Estim (Calcd) %	Total mass loss	Assignment	Residues
H_2L	45-305	225	1	27.21 (27.22)		- Loss of $C_4H_6O_2$.	
	305-535	409	1	25.30 (25.31)		- Loss of $C_4H_4N_2$.	
	535-700	619	1	24.03 (24.05)		- Loss of C_6H_4.	-------
	700-1000	782	1	23.41 (23.42)	99.95 (100)	- Loss of C_6H_2.	
1	25-285	83, 149	2	22.74 (22.96)		- Loss of $2H_2O$, N_2 and HCl.	
	285-415	315	1	13.25 (13.49)		- Loss of $C_4H_3O_{0.5}$.	
	415-590	453	1	14.62 (14.63)		- Loss of C_5H_4.	½ Cr_2O_3+3C
	590-1000	740	1	23.21 (23.32)	73.82 (74.40)	- Loss of C_8H_6.	
2	10-135	79, 100	2	12.26 (12.77)		- Loss of $3H_2O$.	
	135-180	174	1	3.73 (3.78)		- Loss of CH_4.	
	180-245	235	1	6.02 (6.15)		- Loss of C_2H_2.	MnO+8C
	245-670	270, 450	2	21.72 (21.75)		- Loss of C_5H_4 and N_2.	
	670-1000	710	1	15.83 (16.08)	59.56 (60.53)	- Loss of C_4H_4O.	
3	35-295	139	1	22.28 (22.30)		- Loss of $2.5H_2O$, HCl and NH_3.	
	295-680	652	1	25.53 (25.60)		- Loss of C_8NH_3.	½ Fe_2O_3+10C
	680-1000	790	1	6.72 (6.79)	54.53 (54.69)	- Loss of C_2H_6.	

4	10-95	60	1	6.32 (6.33)	- Loss of $1.5H_2O$.	
	95-375	195	1	17.71 (18.04)	- Loss of $1.5H_2O$ and C_4H_2.	CoO+9C
	375-630	608	1	19.13 (19.20)	- Loss of $C_4H_6N_2$.	
	630-1000	750	1	13.39 (13.59) 56.55 (57.16)	- Loss of C_3H_6O.	
5	15-440	80, 240	2	35.10 (35.63)	- Loss of $3H_2O$ and C_8H_2.	
	440-565	520	1	7.43 (7.50)	- Loss of CH_3OH.	NiO+10C
	565-1000	825	1	10.80 (11.25) 53.33 (54.38)	- Loss of CH_4 and N_2H_4.	
6	10-135	94	1	4.44 (4.63)	- Loss of H_2 and H_2O.	
	135-410	162	1	18.75 (18.77)	- Loss of C_2H_7N and $2H_2O$.	CuO+13C
	410-1000	510, 635	2	22.01 (22.02) 45.20 (45.42)	- Loss of C_5H_5NO.	
7	10-140	67	1	4.13 (4.15)	- Loss of H_2O.	
	140-375	268	1	17.75 (17.77)	- Loss of $2H_2O$ and C_2H_3N.	ZnO+10C
	375-1000	392	1	31.59 (31.61) 53.47 (53.53)	- Loss of $C_8H_{11}NO$.	
8	10-225	59	1	5.59 (5.62)	- Loss of $1.5H_2O$.	
	225-485	265	1	13.92 (13.95)	- Loss of $1.5H_2O$ and C_3H_4.	CdO
	485-1000	688	1	53.35 (53.70) 72.86 (73.27)	- Loss of C_3H_4O.	

[a]Numbers are given in Experimental part.

Table 6. Biological activity of H_2L ligand and its complexes[a]

Sample	Inhibition zone diameter (mm / mg sample)						
	Staphylococcus aureus (G^+)	***Bacillis subtilis*** (G^+)	***Salmonella SP.*** (G^-)	***Escherichia coli*** (G^-)	***Pseudomonas aeruginosa*** (G^-)	***Aspergillus fumigatus***	***Candida albicans***
Control: DMSO	0	0	0	0	0	0	0
H_2L	10	14	12	13	17	15	17
1	13	12	15	13	12	17	18
2	9	9	16	9	9	18	19
3	11	11	17	11	11	16	15
4	17	23	18	15	18	24	25
5	13	13	18	13	12	25	20
6	11	13	19	11	11	24	26
7	13	14	17	12	13	18	21
8	15	24	19	15	15	27	28
Ampicillin	23	32	-	-	-	-	-
Gentamycin	-	-	17	19	16	-	-
Amphotericin B	-	-	-	-	-	23	25

[a]Numbers are given in Experimental part.

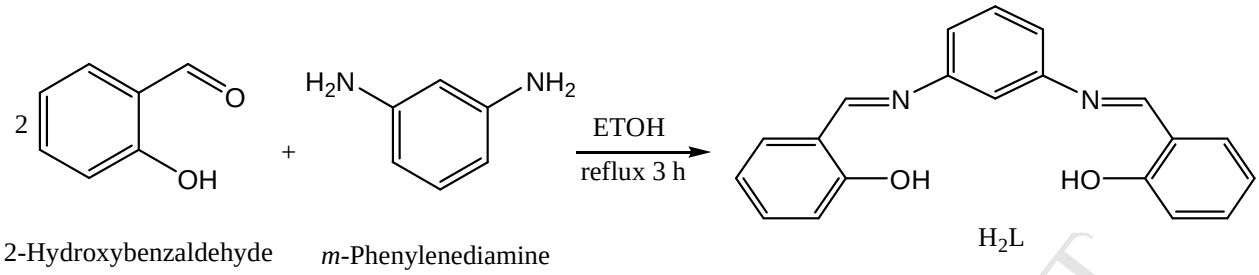

2-Hydroxybenzaldehyde *m*-Phenylenediamine

Scheme 1. Preparation and suggested structure of the tetradentate ligand (H_2L).

3T88

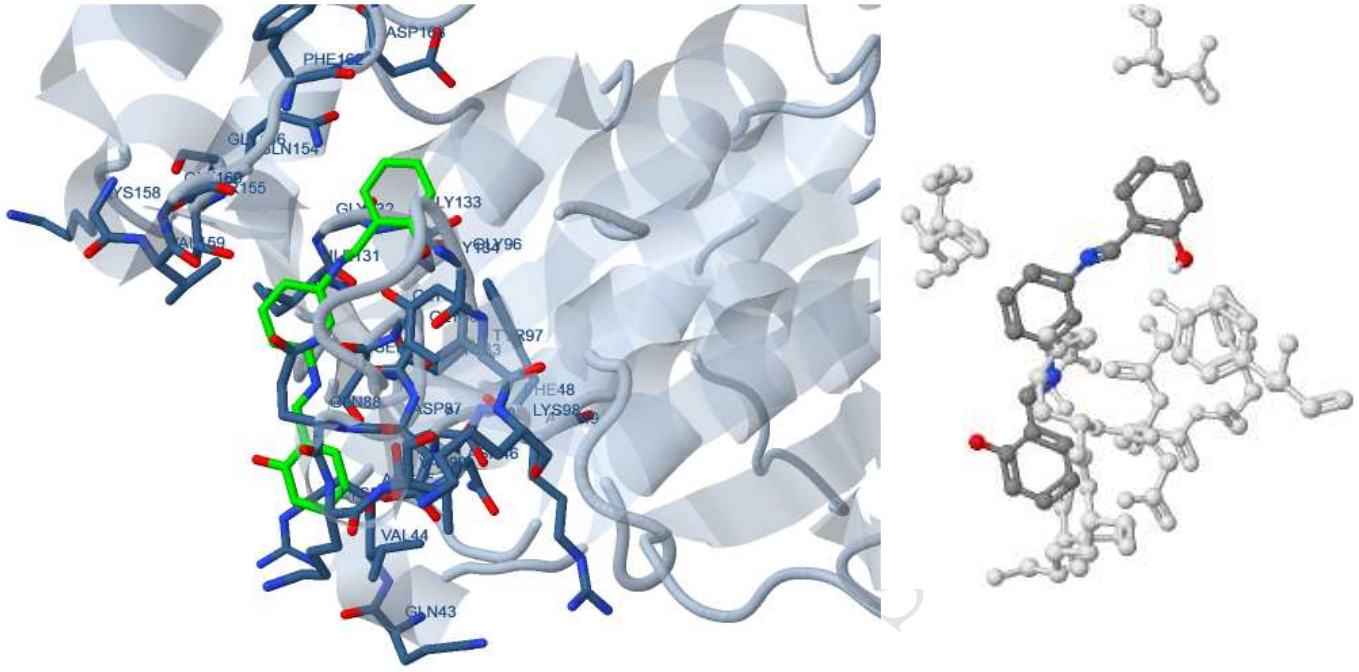

(a) (b)

3Q8U

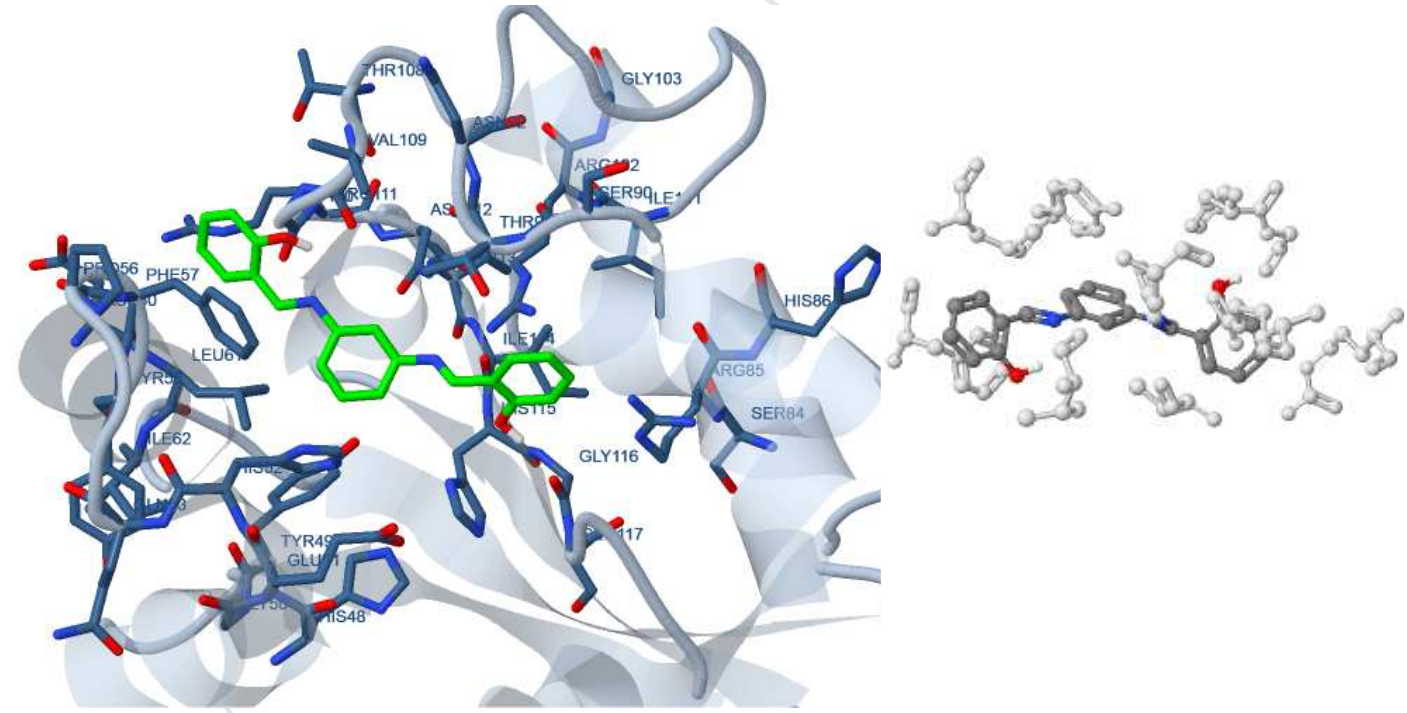

(a) (b)

Fig. 1. The tetradentate ligand (H_2L) (green in (a) and gray in (b)) in interaction with receptors of *Escherichia coli* (3T88) and *Staphylococcus aureu* (3Q8U).

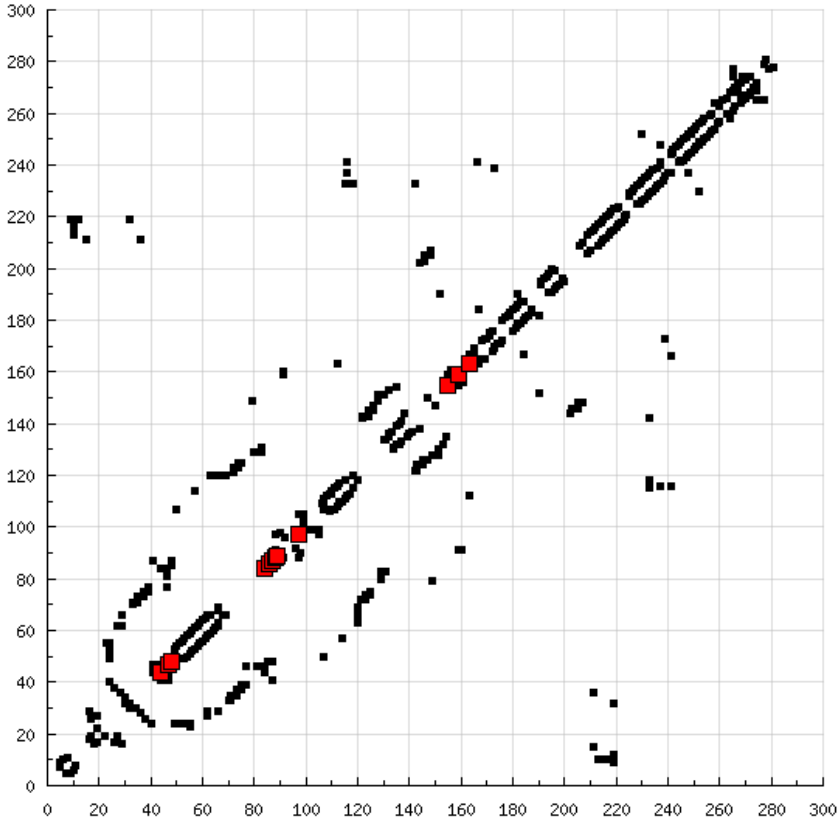

Interactions

44: VAL
47: ALA
48: PHE
84: SER
86: GLY
87: ASP
88: GLN
89: LYS
97: TYR
155: THR
159: VAL
163: ASP

(a)

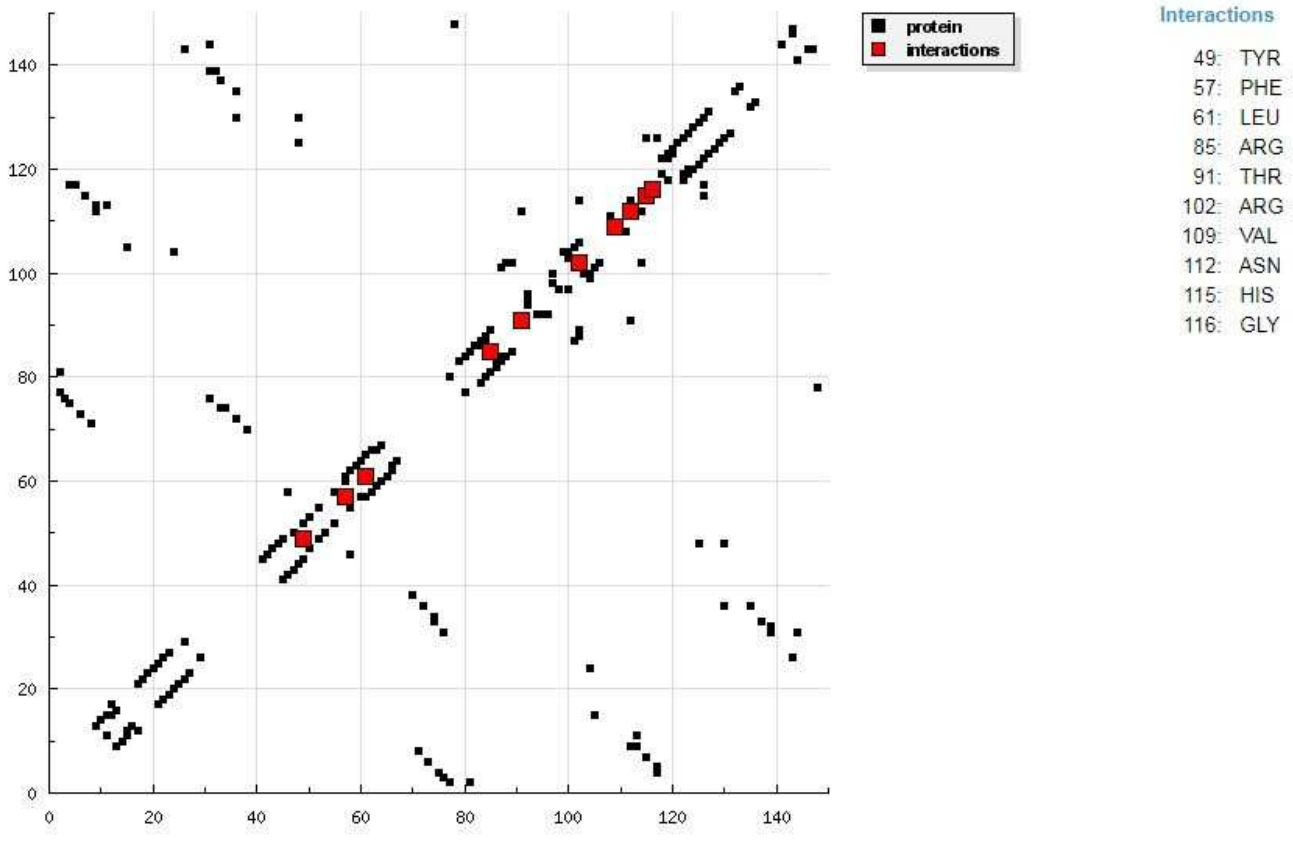

(b)

Fig. 2. HB plot of interaction between the tetradentate ligand (H_2L) and receptors (a) *Escherichia coli* (3T88) and (b) *Staphylococcus aureu* (3Q8U).

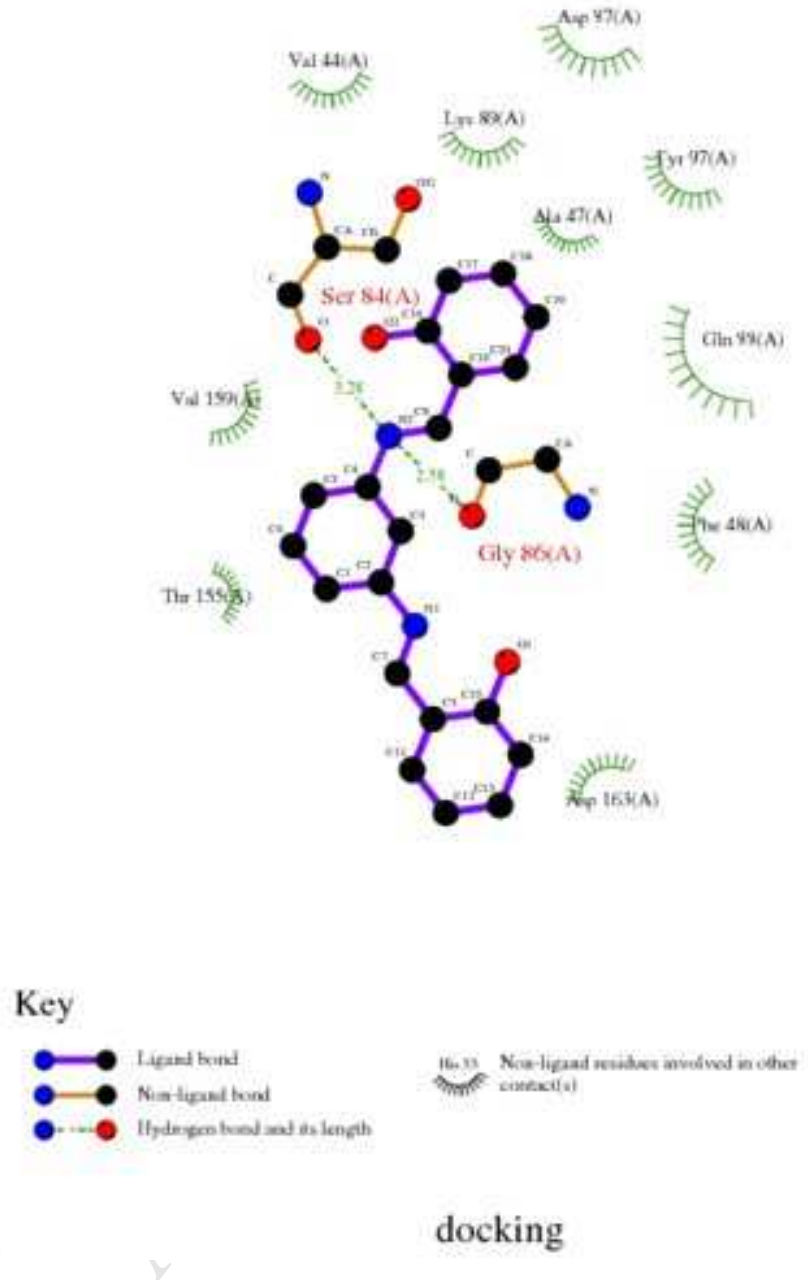
Asp 97(A)
Val 44(A)
Lys 89(A)
Tyr 97(A)
Ala 47(A)
Ser 84(A)
Gln 99(A)
Val 159(A)
Gly 86(A)
Ile 48(A)
Thr 155(A)
Asp 163(A)
Key
Ligand bond
Non-ligand bond
Hydrogen bond and its length
Non-ligand residues involved in other contact(s)
docking

(a)

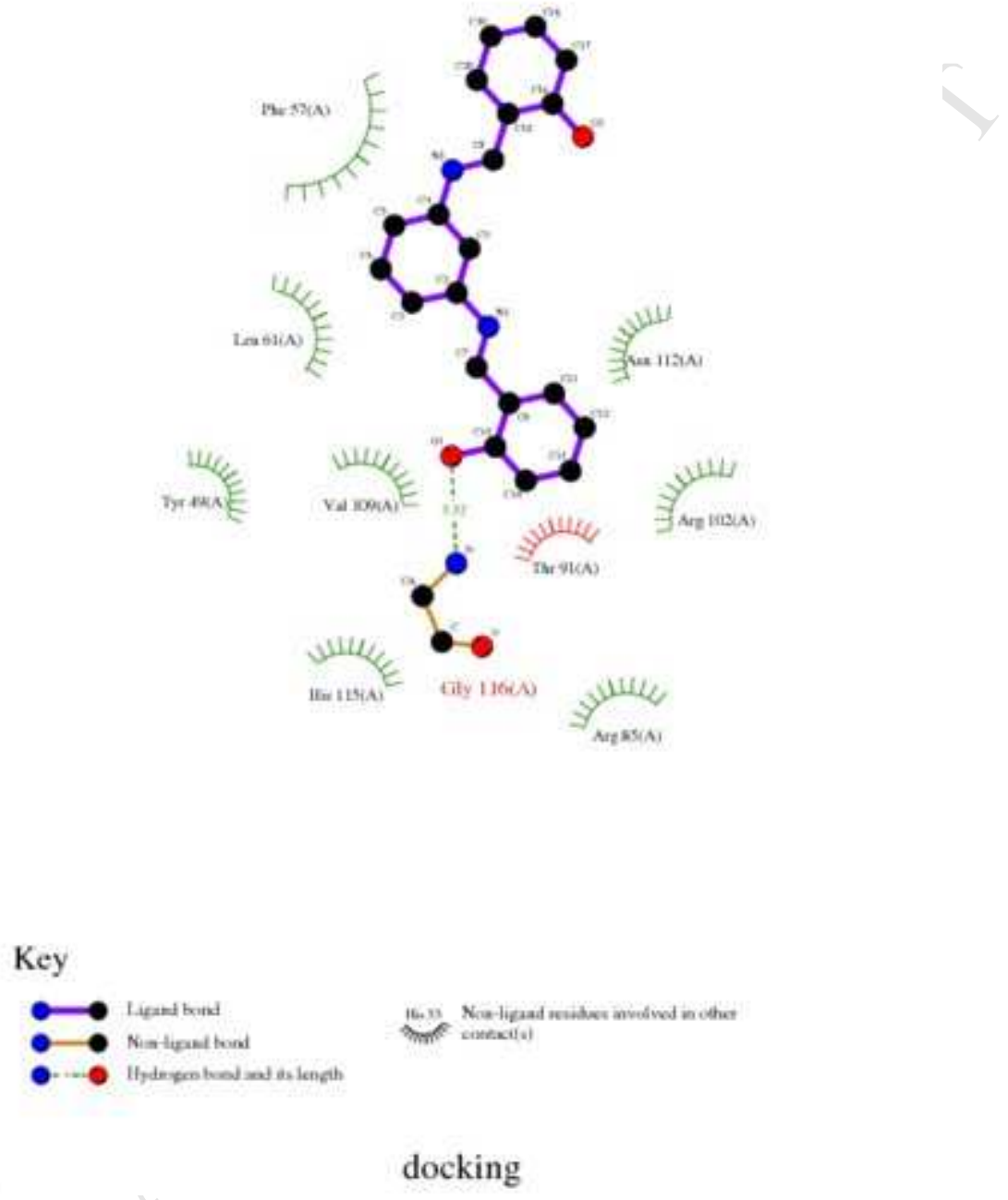

(b)

Fig. 3. 2D plot of interaction between the tetradentate ligand (H_2L) and receptors (a) *Escherichia coli* (3T88) and (b) *Staphylococcus aureu* (3Q8U).

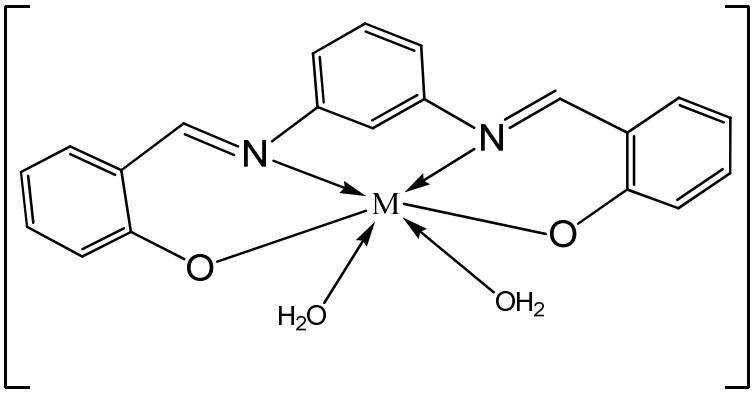

M = Mn, Co, Ni, Cu, Zn, Cd n = 1, x = 0

M = Fe n = 0, x = 1

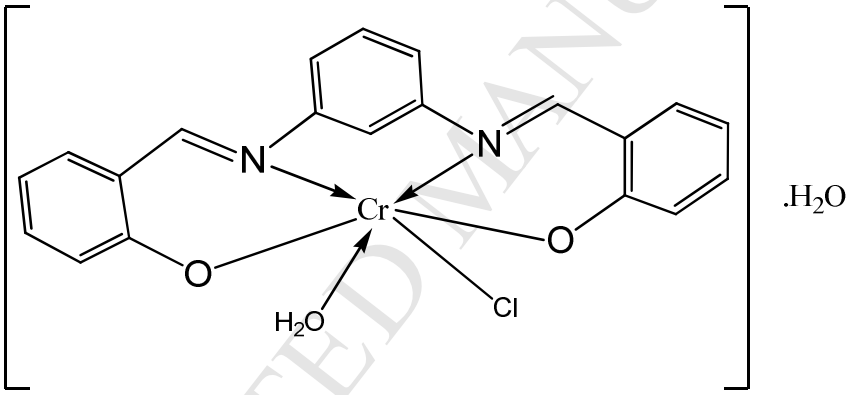

Fig. 4. The structures metal complexes of the ligand (H_2L)**.**

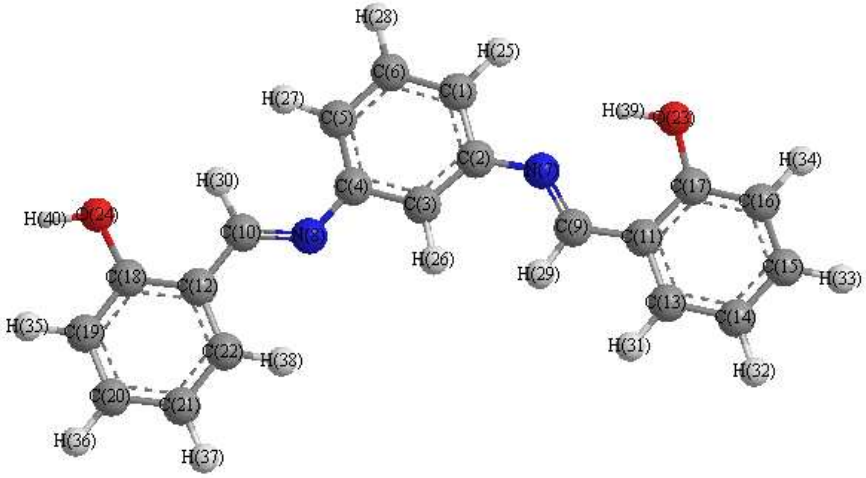

H_2L

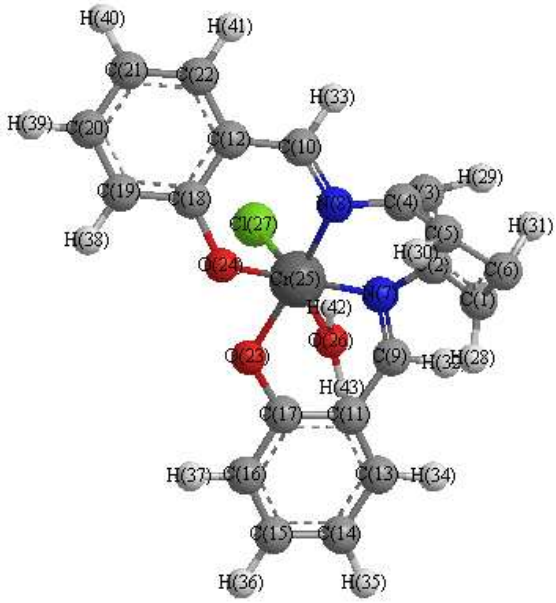

Cr(III) complex (1)

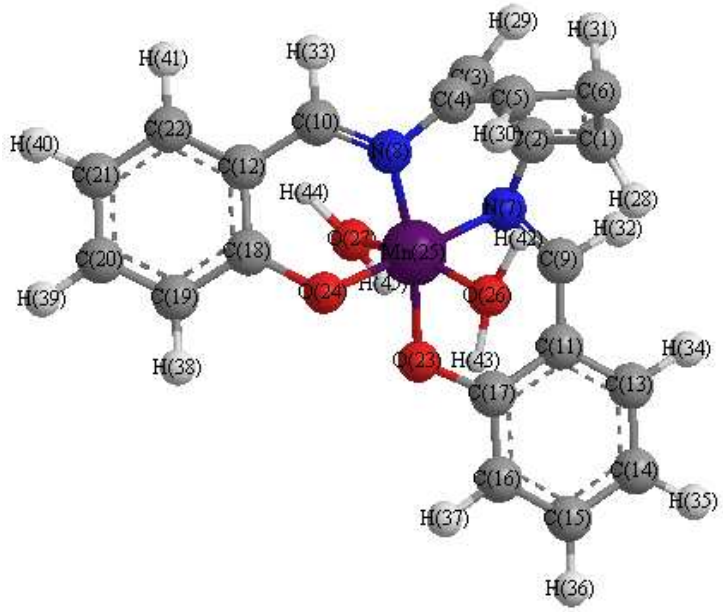

Mn(II) complex (2)

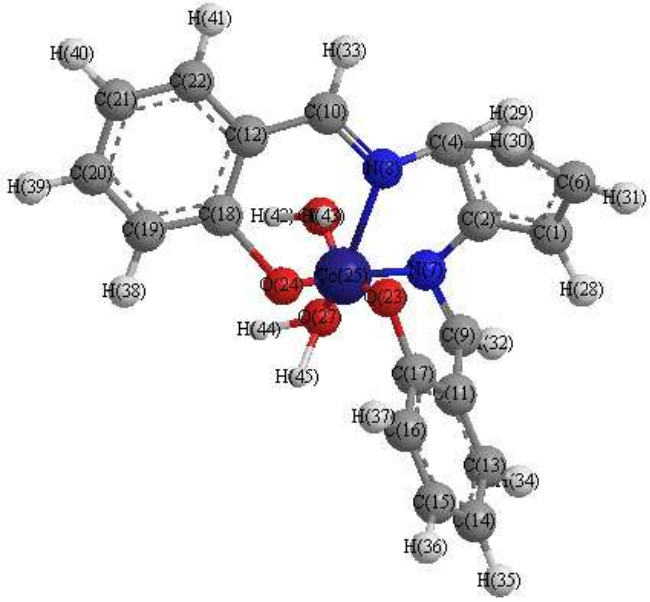

Co(II) complex (4)

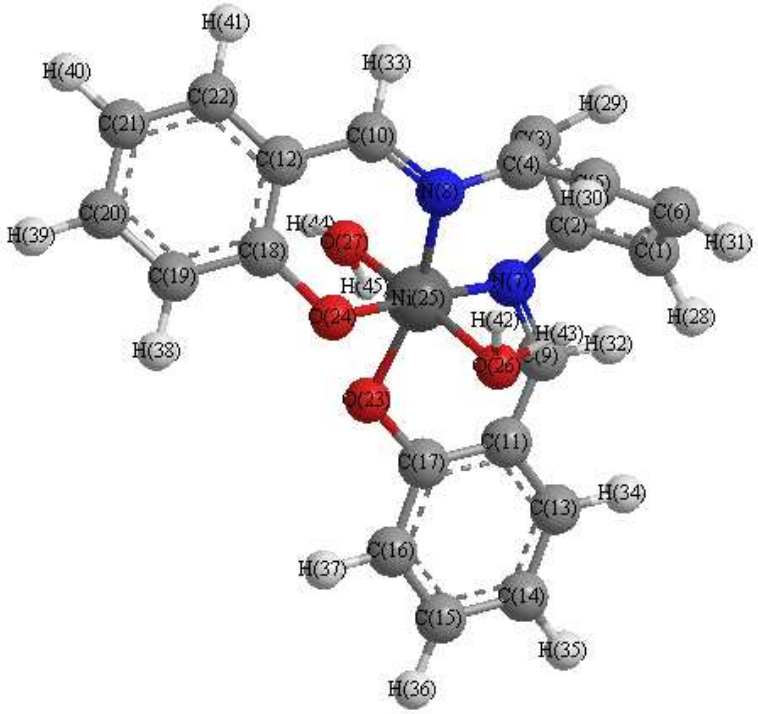

Ni(II) complex (5)

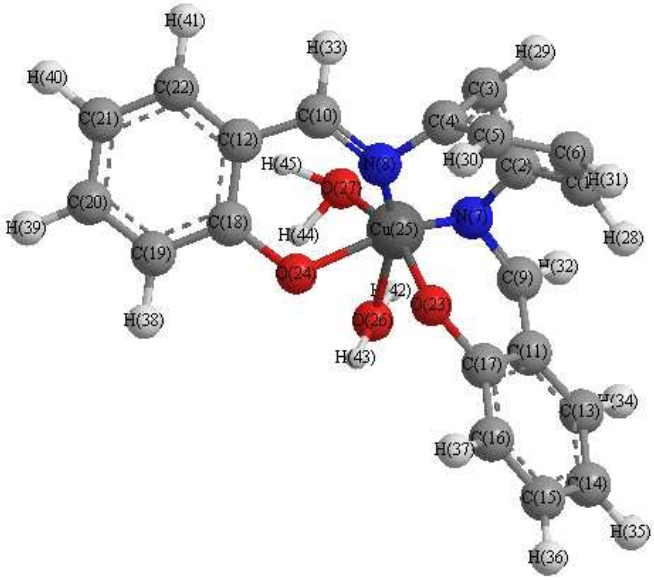

Cu(II) complex (6)

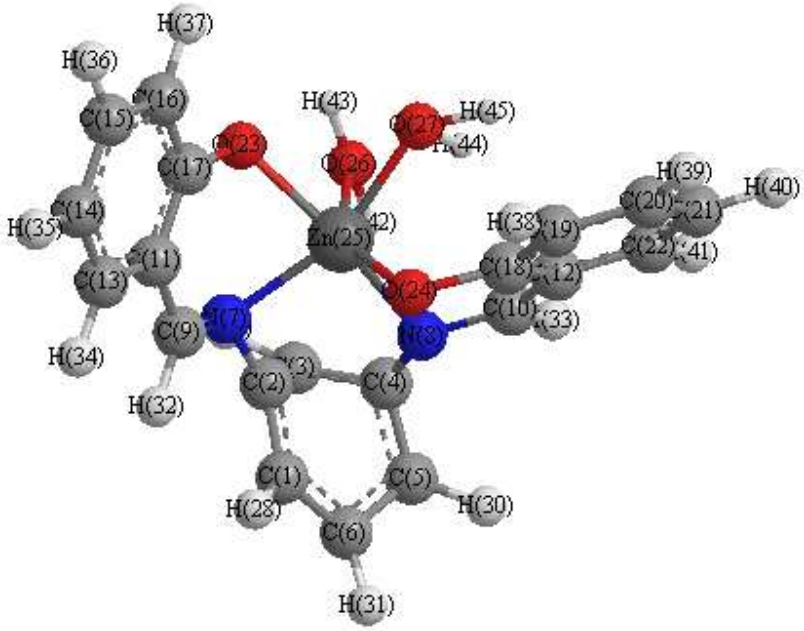

Zn(II) complex (7)

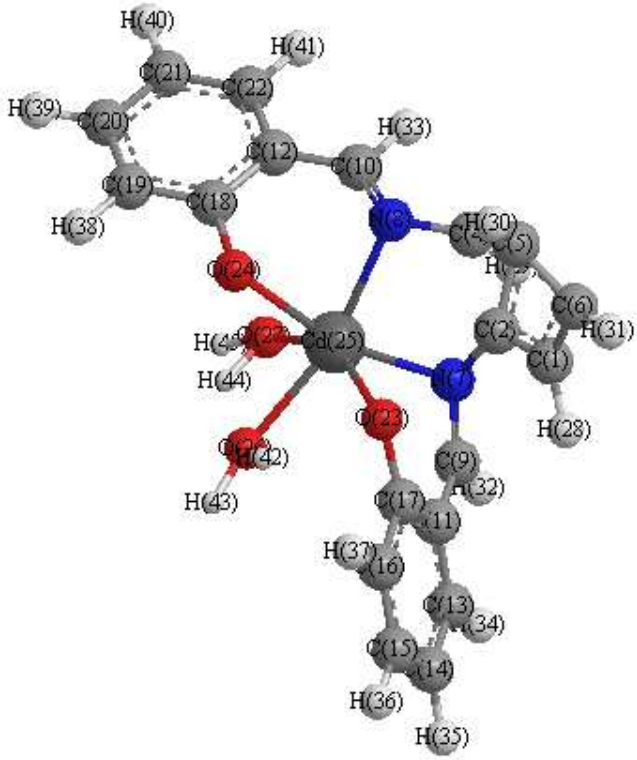

Cd(II) complex (8)

Fig. 5. The optimized structures of the tetradentate ligand (H_2L) and its metal complexes.

	HOMO	LUMO
H_2L	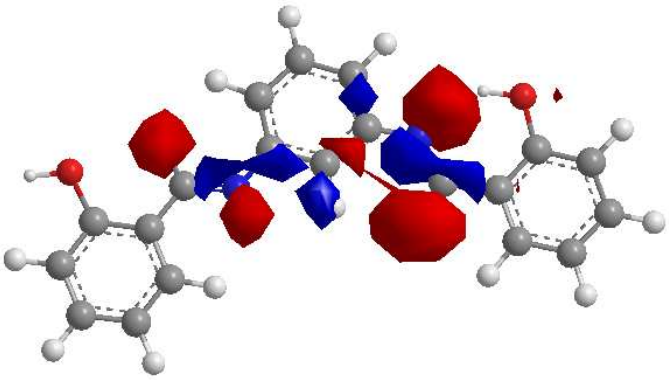	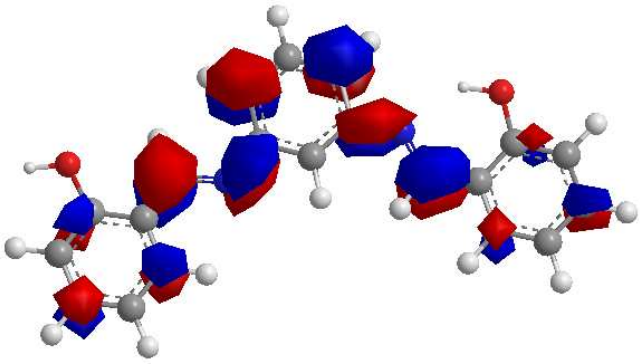
Complex (1)	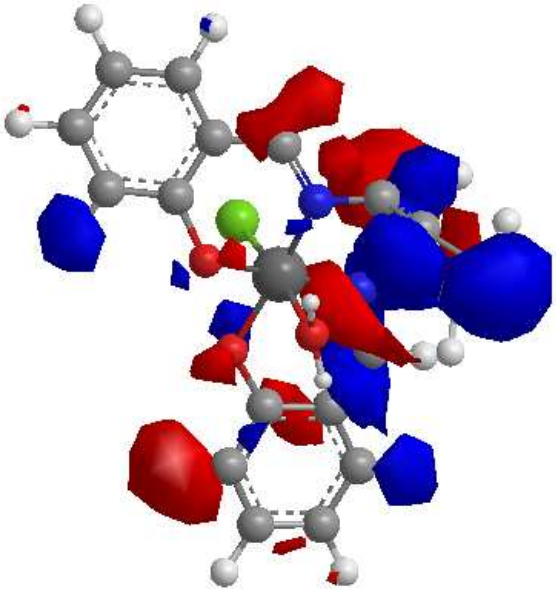	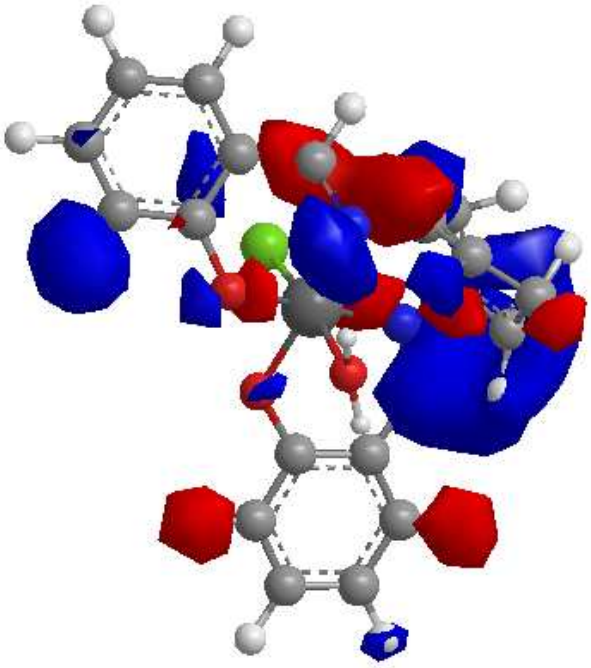

Complex (2)

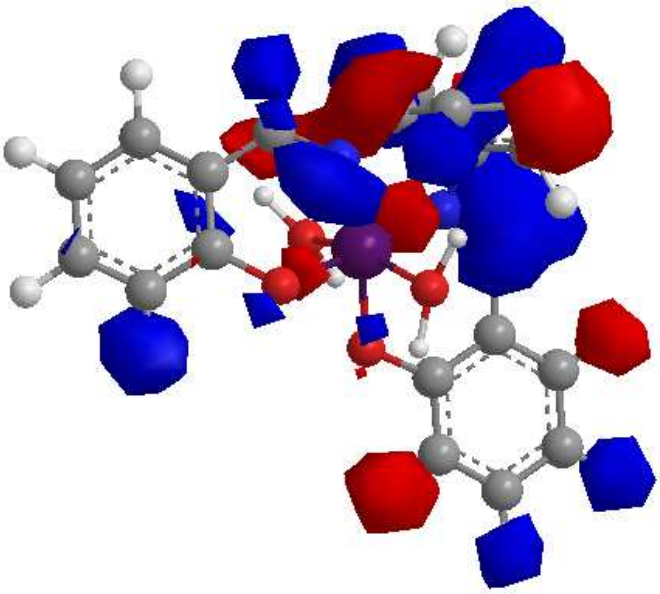

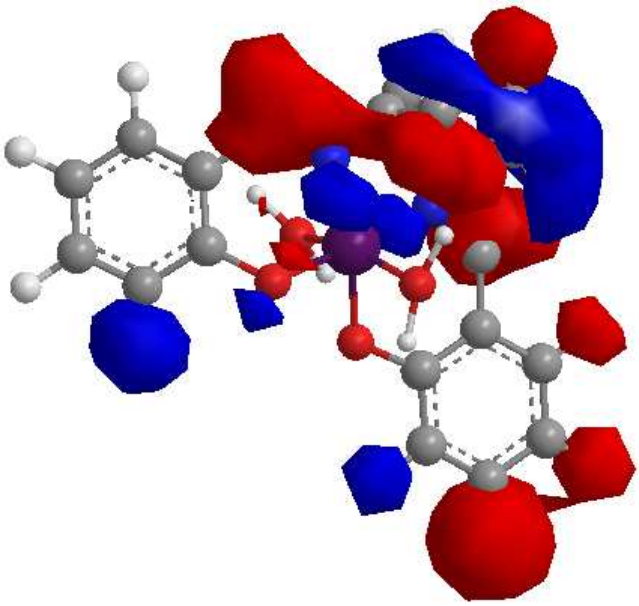

Complex (4)

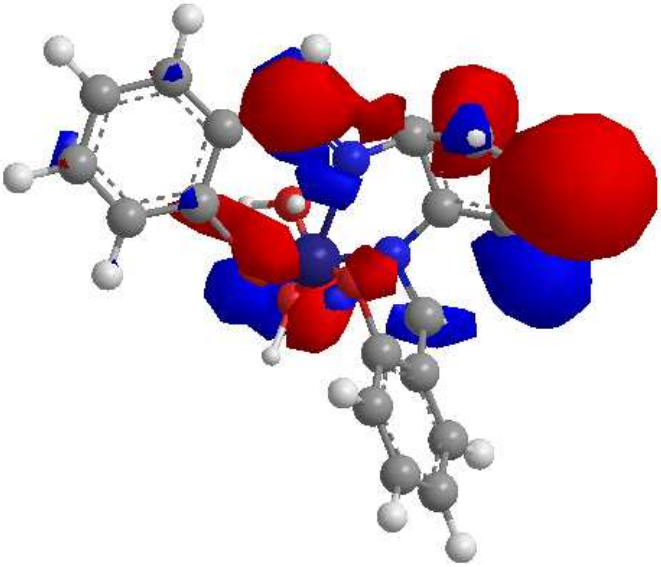

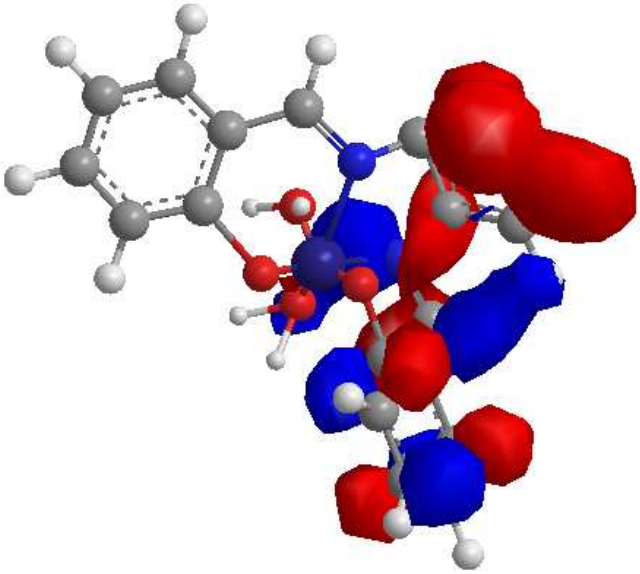

Complex (5)

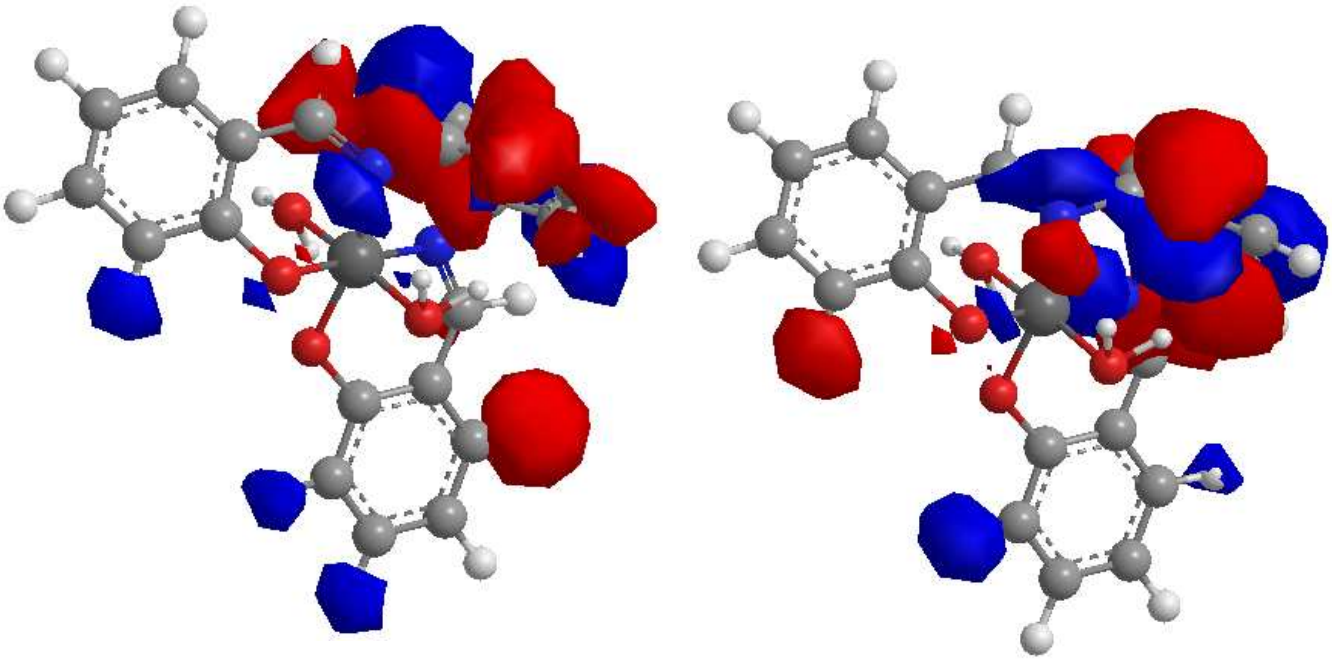

Complex (6)

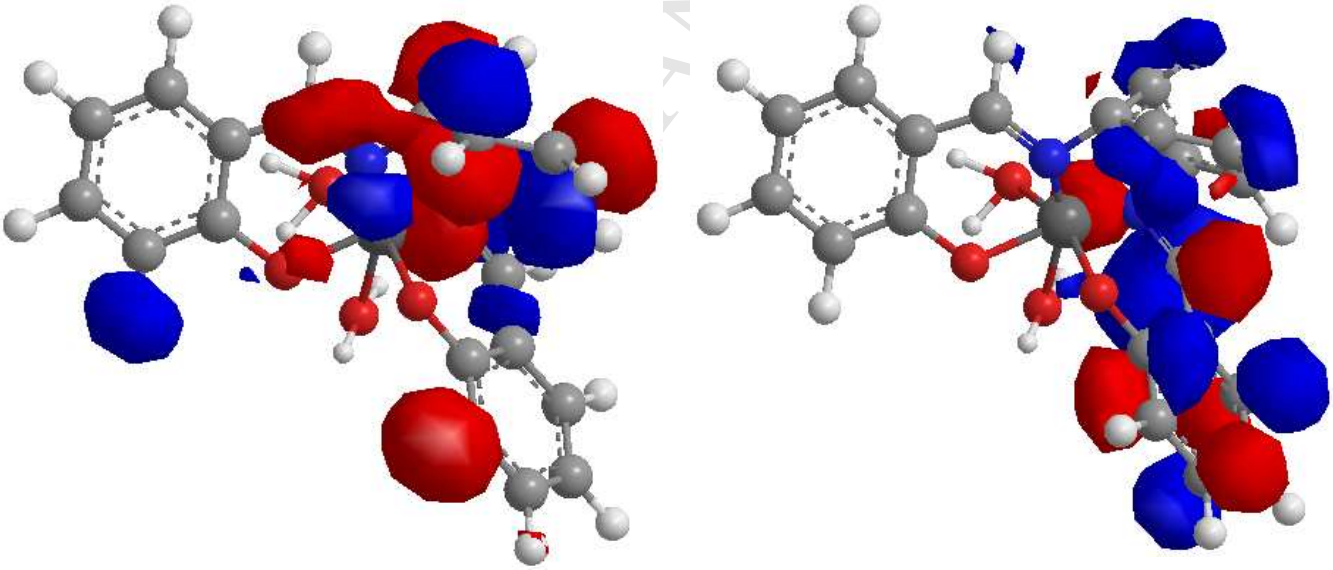

Complex (7)

Complex (8)

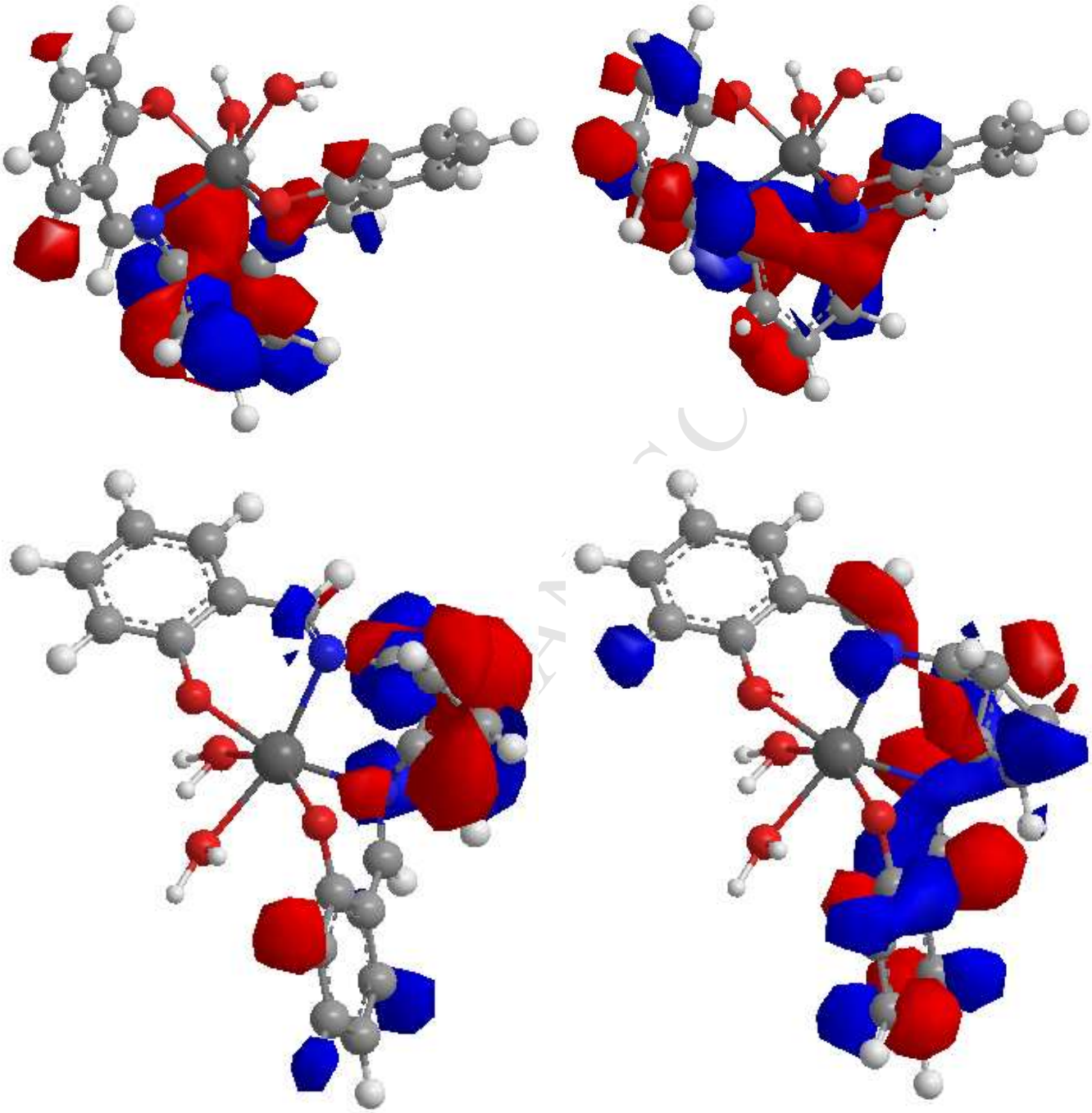

Fig. 6. The highest occupied molecular orbital (HOMO) and the lowest unoccupied molecular orbital (LUMO) of the tetradentate ligand (H_2L) and its metal complexes.

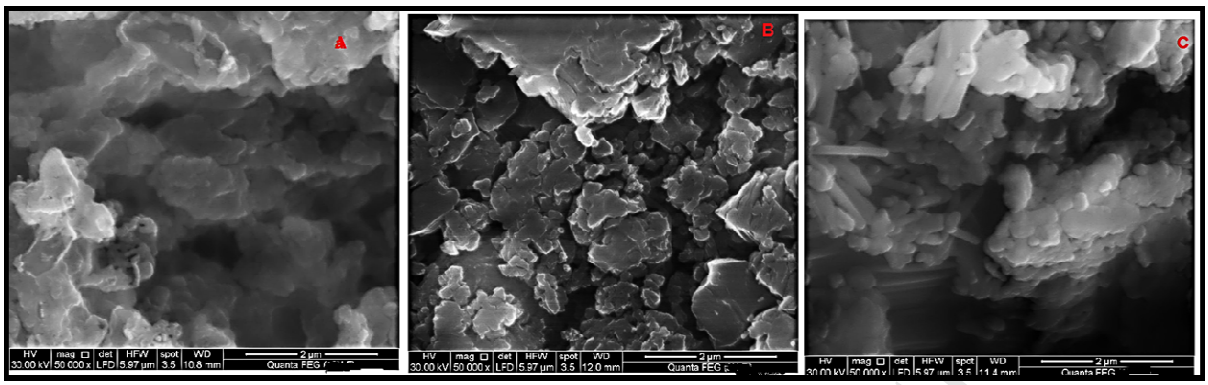

Fig. 7. Scanning electron microscope (SEM) micrographs of A) tetradentate ligand (H_2L), B) Co(II) complex **(4)** and C) Cd(II) complex **(8)**.

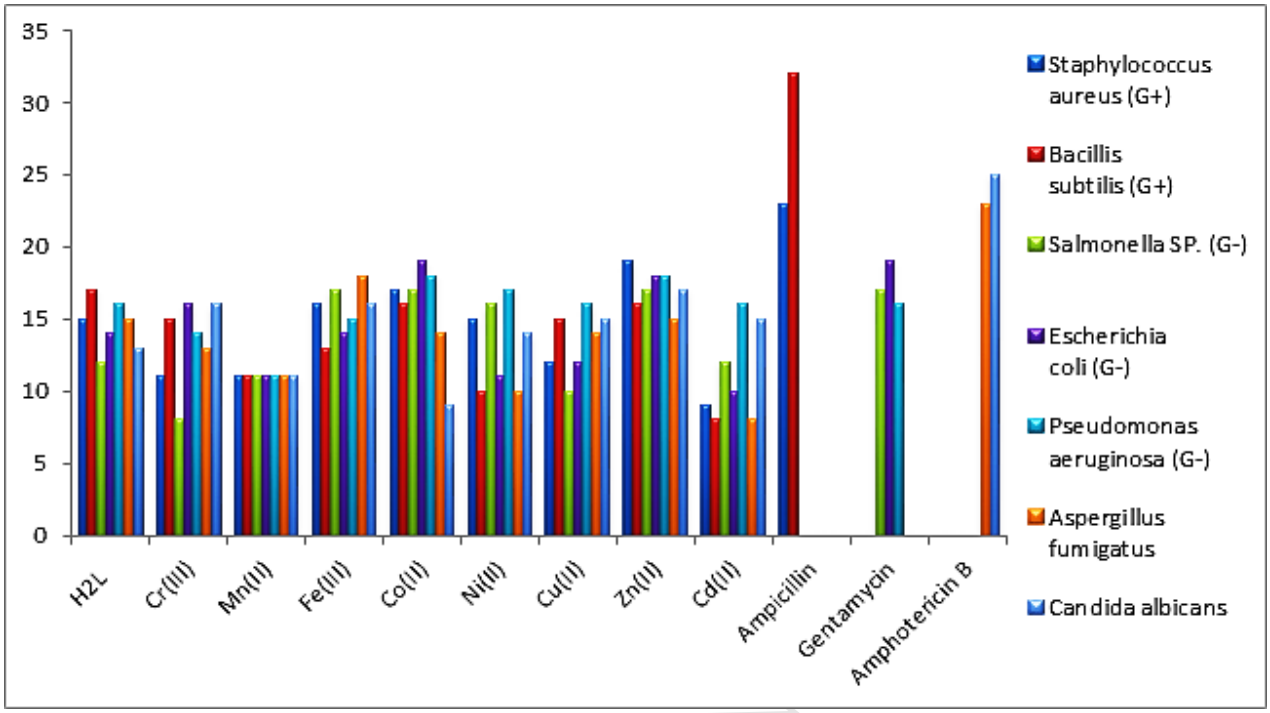

Fig. 8. Biological activity of the ligand (H_2L) and its metal complexes.

- A bi-negative of the ligand and its metal complexes prepared and identified by elemental analysis
- The molecular structures of the ligand and its metal complexes were optimized theoretically
- The quantum chemical parameters of the ligand and its complexes were calculated and discussed
- The compounds were tested for their antimicrobial and antifungal activities
- The calculated binding energy values of the receptors (3T88 and 3Q8U) for ligand